Atmos. Chem. Phys., 18, 10825–10847, 2018
https://doi.org/10.5194/acp-18-10825-2018

Atmospheric Chemistry and Physics
Open Access
EGU

Oxidation processes in the eastern Mediterranean atmosphere: evidence from the modelling of HO_x measurements over Cyprus

Chinmay Mallik[1], Laura Tomsche[1], Efstratios Bourtsoukidis[1], John N. Crowley[1], Bettina Derstroff[1], Horst Fischer[1], Sascha Hafermann[1], Imke Hüser[1], Umar Javed[1], Stephan Keßel[1], Jos Lelieveld[1,2], Monica Martinez[1], Hannah Meusel[3], Anna Novelli[4], Gavin J. Phillips[5], Andrea Pozzer[1], Andreas Reiffs[1], Rolf Sander[1], Domenico Taraborrelli[4], Carina Sauvage[1], Jan Schuladen[1], Hang Su[3], Jonathan Williams[1,2], and Hartwig Harder[1]

[1]Atmospheric Chemistry Department, Max Planck Institute for Chemistry, 55128 Mainz, Germany
[2]Energy, Environment and Water Research Center, Cyprus Institute, Nicosia, 1645, Cyprus
[3]Multiphase Chemistry Department, Max Planck Institute for Chemistry, 55128 Mainz, Germany
[4]Institute of Energy and Climate Research, Forschungszentrum Jülich GmbH, 52425 Jülich, Germany
[5]Department of Natural Sciences, University of Chester, Chester, CH1 4BJ, UK

Correspondence: Hartwig Harder (hartwig.harder@mpic.de) and Chinmay Mallik (chinmay.mallik@mpic.de)

Received: 9 January 2018 – Discussion started: 14 February 2018
Revised: 10 June 2018 – Accepted: 20 June 2018 – Published: 31 July 2018

Abstract. The Mediterranean is a climatically sensitive region located at the crossroads of air masses from three continents: Europe, Africa, and Asia. The chemical processing of air masses over this region has implications not only for the air quality but also for the long-range transport of air pollution. To obtain a comprehensive understanding of oxidation processes over the Mediterranean, atmospheric concentrations of the hydroxyl radical (OH) and the hydroperoxyl radical (HO_2) were measured during an intensive field campaign (CYprus PHotochemistry EXperiment, CYPHEX-2014) in the northwest of Cyprus in the summer of 2014. Very low local anthropogenic and biogenic emissions around the measurement location provided a vantage point to study the contrasts in atmospheric oxidation pathways under highly processed marine air masses and those influenced by relatively fresh emissions from mainland Europe.

The CYPHEX measurements were used to evaluate OH and HO_2 simulations using a photochemical box model (CAABA/MECCA) constrained with CYPHEX observations of O_3, CO, NO_x, hydrocarbons, peroxides, and other major HO_x ($OH + HO_2$) sources and sinks in a low-NO_x environment (< 100 pptv of NO). The model simulations for OH agreed to within 10 % with in situ OH observations. Model simulations for HO_2 agreed to within 17 % of the in situ observations. However, the model strongly under-predicted HO_2 at high terpene concentrations, this under-prediction reaching up to 38 % at the highest terpene levels. Different schemes to improve the agreement between observed and modelled HO_2, including changing the rate coefficients for the reactions of terpene-generated peroxy radicals (RO_2) with NO and HO_2 as well as the autoxidation of terpene-generated RO_2 species, are explored in this work. The main source of OH in Cyprus was its primary production from O_3 photolysis during the day and HONO photolysis during early morning. Recycling contributed about one-third of the total OH production, and the maximum recycling efficiency was about 0.7. CO, which was the largest OH sink, was also the largest HO_2 source. The lowest HO_x production and losses occurred when the air masses had higher residence time over the oceans.

1 Introduction

1.1 Air pollution and HO_x chemistry

The chemical and photochemical processing of air pollutants, in conjunction with local emissions, meteorology, and atmospheric transport, strongly influences the air quality over a region. The regional air quality impacts human health, agriculture, the overall condition of the biosphere, and subsequently the climate. Studies attribute 2–4 million premature deaths globally to outdoor air pollution (Silva et al., 2013;

Lelieveld et al., 2015). Oxidants in the Earth's atmosphere prevent the pollutants released into it from building up to toxic levels. These oxidants not only convert many toxic pollutants into less toxic forms, e.g. carbon monoxide (CO) to carbon dioxide (CO_2), but also help in their removal, e.g. nitrogen oxides (NO_x) and sulfur dioxide (SO_2) are converted into soluble nitric acid (HNO_3) and sulfuric acid (H_2SO_4) respectively, although some toxic chemicals may still be formed during degradation of non-toxic ones. Most of the oxidation processes in the atmosphere proceed along reaction pathways initiated by the hydroxyl radicals (OH) during the day (Levy, 1971), making it the dominant chemical cleaning agent of the daytime atmosphere (Lelieveld et al., 2004). The dominant primary production of OH is via the photolysis of ozone (O_3) at ultraviolet wavelengths (Crosley, 1995), producing electronically excited $O(^1D)$ atoms (Reaction R1). O^1D that escapes quenching (Reaction R2) reacts with water vapour in the atmosphere to produce OH radicals (Reaction R3).

$$O_3 + h\nu \rightarrow O(^1D) + O_2 \quad (R1, \lambda < 330\,\text{nm})$$

$$O(^1D) + M \rightarrow O(^3P) + M(M = N_2, O_2) \quad (R2)$$

$$O(^1D) + H_2O \rightarrow 2OH \quad (R3)$$

Because OH reacts rapidly with several biogenically and anthropogenically emitted gases (e.g. Reaction R4), its lifetime is typically a few hundred milliseconds in the troposphere. Oxidation limits these gases (methane (CH_4), CO, volatile organic compounds (VOCs)) from accumulating above trace levels in the troposphere. Reactions of OH with CO and hydrocarbons (HCs) (Reaction R4) also trigger quasi-instant formation of the hydroperoxyl radical (HO_2, via Reaction R5) in our O_2-rich atmosphere. In the presence of nitric oxide (NO) and O_3 (Reactions R6, R7), a chemical equilibrium is set between OH and HO_2 on a timescale of seconds. The sum of OH and HO_2 is known as HO_x. The Reactions (R6) and (R7) maintain the oxidizing efficiency of the atmosphere by recycling OH. Simultaneously, in the presence of NO_x ($= NO +$ nitrogen dioxide (NO_2)), they also propel a reaction chain leading to O_3 formation via Reactions (R8) and (R9). Reactions (R8)–(R9) are the main chemical source of tropospheric O_3, which is an important oxidant, a greenhouse gas, and a major secondary pollutant.

$$CO + OH \rightarrow CO_2 + H \quad (R4)$$

$$H + O_2(+M) \rightarrow HO_2(+M) \quad (R5)$$

$$NO + HO_2 \rightarrow NO_2 + OH \quad (R6)$$

$$HO_2 + O_3 \rightarrow OH + 2O_2 \quad (R7)$$

$$NO_2 + h\nu \rightarrow O(^3P) + NO(\lambda < 430\,\text{nm}) \quad (R8, \lambda < 430\,\text{nm})$$

$$O(^3P) + O_2(+M) \rightarrow O_3(+M) \quad (R9)$$

OH also oxidizes anthropogenic and biogenic HCs emitted into the atmosphere, leading to peroxy radicals (RO_2). NO converts the RO_2 into HO_2, which again leads to OH recycling (Reaction R6). The HO_x cycle can be terminated by the radical+radical interactions of RO_2 and HO_2 with and among themselves to form peroxides (Reactions R10 and R11). Depending on NO levels, the RO_2 species can react through different channels. Under low-NO_x conditions, e.g. in the clean marine boundary layer, when the reaction of RO_2 with NO is less significant than its reaction with HO_2, peroxide formation becomes a major sink for HO_2, further leading to OH and O_3 removal. Under higher NO levels, RO_2 would react with NO to form NO_2 (O_3 source), HO_2 (OH source), alkyl nitrates, and aldehydes (Reactions R12, R13, and R14). Further, there have been suggestions of autooxidation of RO_2 to produce peroxides, yielding OH under atmospheric conditions (Crounse et al., 2013). These autooxidation mechanisms proceed through catalytic H shifts at a very fast rate (up to $\sim 0.1\,s^{-1}$), e.g. conversion of RO_2 generated from a carbonyl compound into a highly functionalized dicarbonyl hydroperoxide compound (Reaction R15).

$$HO_2 + HO_2 \rightarrow H_2O_2 + O_2 \quad (R10)$$

$$RO_2 + HO_2 \rightarrow ROOH + O_2 \quad (R11)$$

$$RO_2 + NO + O_2 \rightarrow R'CHO + HO_2 + NO_2 \quad (R12)$$

$$RO_2 + NO \rightarrow RNO_3 \quad (R13)$$

$$NO_2 + OH + M \rightarrow HNO_3 + M(M = N_2, O_2) \quad (R14)$$

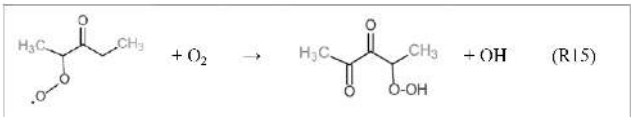

(R15)

In polluted air when NO_x concentrations become large enough that the reaction of NO_2 with OH dominates over other HO_x sinks, the major loss of HO_x is via the formation of nitric acid (HNO_3, Reaction R14), which is then removed from the atmosphere by wet and dry deposition. Some acid-forming reactions are also the starting point of particle formation in the atmosphere, e.g. via oxidation of SO_2. In sum, oxidation is a means by which major pollutants are processed and removed from the atmosphere, but with concomitant implications for air quality, agriculture, climate, and health. However, large uncertainties in atmospheric reaction pathways, rate coefficients, and measurements of atmospheric gases and radicals limit our ability to understand and predict the quality of ambient air.

1.2 Motivation for the campaign

The Mediterranean is a climatically sensitive region which is rapidly getting warmer and dryer over time (Lelieveld et al., 2012). The atmospheric chemistry over the region is complex, with regular exceedances of the European Union (EU) ozone air quality standard (Doche et al., 2014; Kalabokas et al., 2013) and a projected increase in summertime O_3 over the eastern Mediterranean (Lelieveld et al.,

2002; Lelieveld and Dentener, 2000). Cyprus is a small, remote island (area: 9251 km^2; population: 1.15×10^6; density: 119.2 people km^{-2}) in the eastern Mediterranean (south of mainland Europe) with very low local emissions. The nonmethane volatile organic compounds (NMVOCs), NO_x, and SO_x emitted by Cyprus and the European Union (EU28) were 6.8, 17.2, and 16.8 Gg and 6722, 7819, and 3083 Gg respectively for 2014 (European Union emission inventory report, 2017). Being located downwind of the mainland Europe emissions, Cyprus provides an ideal vantage point to study the impact of European emissions on the Mediterranean climate (Lelieveld et al., 2002). To study the atmospheric chemistry over the Mediterranean and understand the impact of emissions from different regions of Europe on air quality in Cyprus, an intensive field measurement campaign (the Cyprus Photochemistry EXperiment, hereafter CYPHEX) was conducted in Cyprus during the summer of 2014, wherein a comprehensive suite of trace gases was measured.

Cyprus is exposed to air masses influenced by emissions from southwestern European countries that are photochemically processed over the Mediterranean Sea. The Etesian winds during summer carry air masses loaded with emissions from industry and biomass burning over central and eastern European countries. Although emissions from Europe have been steadily decreasing over the past few decades (e.g. NO_x, SO_x, and NMVOCs decreased by nearly 50 %, 80 %, and 57 % respectively during 1990–2013; European Union emission inventory report, 2017), these emissions are still substantial with respect to the global total. Apart from the influence of European emissions, Cyprus is strategically located at a crossroads of air masses from Asia, Africa, and the Atlantic (Kleanthous et al., 2014). Influence from all these different source regions, incorporating the impact of a plethora of HCs, nitrogen and sulfur species, and mineral dust on the atmospheric processing in this part of the world, has attracted several field campaigns (Carslaw et al., 2001; Berresheim et al., 2003). For example, the Mediterranean Intensive Oxidant Study (MINOS) was conducted to study the budget of atmospheric oxidants influenced by long-range transport of pollution in the summer of 2001 (Lelieveld et al., 2002; Gros et al., 2003; Salisbury et al., 2003). OH radicals were measured in the coastal boundary layer of Crete as part of the MINOS campaign and the major sources of OH were found to be photolysis of O_3 and recycling from $HO_2 + NO$ reaction (Berresheim et al., 2003). Although HO_2 was not measured during MINOS, high levels of formaldehyde (HCHO), a major primary HO_2 source, were observed (Kormann et al., 2003). In the present study, we report simultaneous measurements of OH and HO_2 during the CYPHEX campaign and compare these observations with simulations from a photochemical box model constrained with O_3; CO; NO; NO_2; peroxides; several anthropogenic and biogenic HCs including important alkanes, alkenes, alkynes, aldehydes, and acids; and photolysis frequencies of important gases relevant to HO_x chemistry. The main objective of this study is to identify the major chemical species and reaction pathways controlling the HO_x chemistry over this climatically sensitive region.

2 Methods

2.1 Measurement site

The CYPHEX campaign was conducted at the northwest coast of Cyprus, on a hilltop about 650 m a.m.s.l., in Paphos District of the island and facing the sea about 5–8 km away on the west. The Akamas Peninsula National Park is about 25 km to the northwest of the measurement site (34°57′ N, 32°23′ E), with terrain descending rapidly to the northeast towards the town of Polis, with a population of about 2000. The area comprises spare shrub-type vegetation with small Mediterranean trees comprising pines, junipers, olives, carob, pomegranates, and almonds. The area is weakly populated in a radius of about 20 km. The site is away from the major cities: Paphos with 90 000 people is 20 km south, Limassol with 235 000 people is 70 km southeast, Larnaca with 145 000 people is 110 km east, and Nicosia with 325 000 people is 90 km northeast (census of population October 2011; www.cystat.gov.cy, last access: 28 December 2017). The local wind direction is predominantly southwest (70 % between 202.5° and 247.5°) (Meusel et al., 2016; Derstroff et al., 2017), bringing in humid air from the sea, with no immediate anthropogenic influence. Analysis of 5-day back trajectories show mainly two major air mass regimes (Hüser et al., 2017). Etesian winds influenced by fresh emissions from eastern–central Europe crossing Turkey and Greece, and mistral winds influenced by emissions from southwestern Europe but processed for a longer period over the Mediterranean (Fig. 1). During the summer of 2014, a weakened east–west pressure gradient led to weak and delayed Etesian winds (Tyrlis et al., 2015). The site is also influenced by local land–sea breezes.

2.2 HO_x measurements during CYPHEX

Atmospheric OH and HO_2 were measured during CYPHEX using the HydrOxyl Radical measurement Unit based on fluorescence Spectroscopy (HORUS) instrument (Martinez et al., 2010). The set-up was based on the well-established laser-induced fluorescence – fluorescence assay by gas expansion (LIF-FAGE) technique for atmospheric OH measurements (Brune et al., 1995; Crosley, 1995; Hard et al., 1984). The laser system consisted of a tunable dye laser, which was pumped by a diode-pumped Nd:YAG laser (Navigator I J40-X30SC-532Q, Spectra Physics) pulsing at 3 kHz. The two laser assemblies were mounted on either side of a vertical plate, which was mounted on a rack inside a measurement container with dimensions of 6 m × 2.5 m × 2.5 m. The output laser radiation was split into a 9 : 1 ratio using

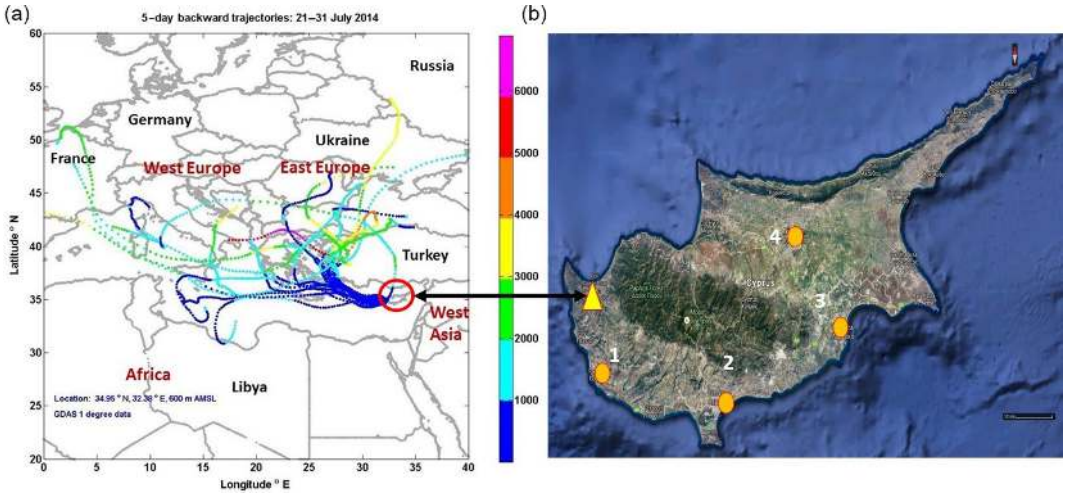

Figure 1. (a) Air masses during CYPHEX; the colour bar represents trajectory height in metres above mean sea level. **(b)** Map of Cyprus. Measurement site (yellow triangle), cities (circles; 1. Paphos, 2. Limassol, 3. Larnaca, 4. Nicosia).

beam splitters, and channelled through 8 m optical fibers into the detection module for measurements of OH and HO_2.

The detection system was mounted about 6 m above ground level (a.g.l.) on the top of a scaffolding tower, constructed close to the wall of an air-conditioned container adjacent to the laser unit. The container with the HORUS instrument was mounted on top of another similar measurement container with O_3, CO, NO_x, and peroxide instruments inside. The inlets for all the instruments measuring during CYPHEX were placed within 5 m of the HORUS detection unit on the tower. Ambient air was drawn in HORUS through a critical orifice with a pinhole size of 0.9 mm into a detection cell with about 4.3 mbar of pressure. This internal pressure was achieved by using a combination of a roots blower (M90 compressor from Eaton, USA) followed by a scroll pump (XDS35i, Edwards, USA). The resulting high volume flow ensured that the exchange of air illuminated by the laser is fast enough between two consecutive pulses, thus avoiding possible laser-induced interferences.

The interaction of the ambient air with the laser beam in the low-pressure detection cell was maximized using a White cell set-up, in which the laser light was reflected 32 times across the detection volume. The OH molecules were selectively excited by a 308 nm laser light pulsing at 3 kHz on resonance with the Q_1 (2) transition line ($A^2\sum -X^2\prod$, $v' = 0 \leftarrow v'' = 0$). An etalon controlled by a stepper motor, in the dye laser set-up, caused the laser radiation to be tuned on and off resonance with the OH transition every 7 s to account for the OH fluorescence plus background signals and the background signals respectively, resulting in a time resolution of 14 s. The spectra from a reference cell, in which OH was produced by H_2O thermolysis, was used to detect the Q_1 (2) line. The counts from the reference cell were used to sustain the on-resonance position while the etalon tethered around it. Although the pressure reduction in the detection cell results in smaller numbers of OH molecules, it improves the OH fluorescence quantum yield due to reduced collisional quenching of excited OH radicals. The lifetime of the excited OH extends beyond the Mie scattering by aerosols and the Raleigh scattering by smaller molecules/particles. These interfering background signals were discriminated by using time-gated microchannel plate detectors (Hamamatsu), enabling excitation of OH radicals and detection of fluorescence at the same wavelength. The excitation at 308 nm is advantageous to the excitation at 282 nm as interference from laser-generated OH due to O_3 photolysis is ~ 25 times smaller at 308 nm. A band-pass filter with a central wavelength of 308 ± 0.75 nm and bandwidth of 5 nm (full width at half maximum, FWHM) in front of the detector prevented signals due to any interfering wavelengths from registering on the detector. The fluorescence decay was recorded with a time resolution of 4 ns and integrated for on-resonance and off-resonance periods, thus delineating the signal from the spectroscopic background. Further, the spectra of the measured atmospheric OH were compared with the one obtained from a reference cell ensuring no interferences from fluorescence of species like SO_2 and naphthalene.

The chemical background, originating from OH being internally produced during the transit time of about 3 ms from the orifice to the centre of the detection cell, was accounted for by removing ambient OH with an OH scavenger. This scavenger, 3–5 sccm of pure propane in a carrier flow of 8000 sccm synthetic air for CYPHEX, was introduced through an inlet pre-injector (IPI) mounted on top of the inlet nozzle (Novelli et al., 2014a; Hens et al., 2014). The scavenger amount was just sufficient to scavenge off ~ 95 % of atmospheric OH as determined from propane titration experiments on site. IPI was connected to a blower that draws about 180–200 L min^{-1} of ambient air from the top of the IPI, the flow being monitored by a differential pressure sensor. The

OH scavenger was injected via eight 0.5 mm diameter holes 5 cm above the pinhole of the OH inlet into the centre of the air flow sampled by the IPI close to its hyperbolic minima (Novelli et al., 2014b). The hyperbolic internal shape of the IPI (maximum cross section of 35 mm and minimum cross section of 6 mm) helps to sample air that has minimum wall contact and flows at a high velocity through a small diameter, ensuring that the scavenger is well mixed with atmospheric air. The high flow also ensures minimum impact of the horizontal wind speed on the mixing efficiency. The IPI cycling was automated by a script resulting in repeated cycles of scavenger injection, flushing, and no injection. The scavenger was periodically injected every 2 min, resulting in alternating measurements of background OH and total OH, i.e. with and without scavenger injection. The difference between these two signals gives a measure of the atmospheric OH with a time resolution of 4 min. The wall losses in the IPI were periodically determined by physically dismounting the IPI for 5 min during measurements during different times of the day. On average, the background signal was 45 % of the total signal during the daytime (Fig. S1 in the Supplement). While the constituents of background OH can have a pronounced impact on atmospheric oxidation processes, especially over regions with high biogenic emissions (Mauldin et al., 2012), the study of the influence of background OH on oxidation pathways during CYPHEX is beyond the scope of the present study.

Atmospheric HO_2 was measured in a detection cell located 16 cm below the OH detection block. HO_2 measurements were achieved by injecting NO purified through a sodium hydroxide-coated silica (Sigma-Aldrich Ascarite) using a 1/8 in. OD, 0.035 in. ID coiled stainless steel loop with a diameter of about 3 cm, placed just above the HO_2 detection block. The NO was injected through 0.1 mm holes, leading to conversion of HO_2 into OH and detected by the same principle as in the first block. To minimize impact of RO_2 on OH formation (Fuchs et al., 2011; Hens et al., 2014), only about 30 % of atmospheric HO_2 was converted to OH using NO. The required NO flow, about 0.5 sccm of pure NO in 10 sccm of carrier flow during CYPHEX, was determined from titrations in ambient and calibration air. Further, tests were carried out with and without NO to ensure that there was no influence of HO_2 conversion on OH in the first axis. The measurement in the HO_2 detection cell yields the total HO_x ($OH + HO_2$). HO_2 is calculated as the difference between HO_x and the OH measured in the first axis, after accounting for the relative OH sensitivities of the two detection axes.

Due to low OH reactivity during CYPHEX, we expect the RO_2 production from the oxidation of HCs to be low. Hence the interference due to potential conversion of atmospheric RO_2 radicals into HO_2 radicals due to the NO injected to convert HO_2 into OH in the low-pressure detection volume is expected to be low compared to regions with high OH reactivities like the boreal forest in Finland. In order to reduce the conversion of RO_2 to HO_2, we used a reduced NO flow of 0.5 sccm resulting in $\sim 7 \times 10^{12}$ cm^{-3} of NO in the detection cell, thus converting only about 30 % of HO_2 radicals to OH radicals while simultaneously reducing the RO_2–HO_2 conversion efficiency. We did not conduct experiments to measure the conversion efficiencies of all possible RO_2 radicals in the atmosphere. To estimate the potential interference due to RO_2 radicals on our measured signal, we made model calculations using CAABA/MECCA in which most of the RO_2 radicals from higher HCs directly form HO_2 radicals after reaction with NO, skipping the reaction step of alkoxy radicals with O_2, which is slower at reduced pressure inside the instrument compared to ambient atmosphere.

The model is run at ~ 4 hPa to see how OH and HO_2 radicals evolve with time in the low-pressure detection volume at different NO concentrations and is validated for calibration conditions (manuscript under preparation). The RO_2 radicals in the model are initialized with the concentrations generated from the model run for the base case (case III in Fig. 3) for our study while OH and HO_2 radicals are initialized with measured concentrations. In Fig. S2a, we show the evolution of OH and HO_2 radicals inside the detection cell after injection of NO ($t = 0$) for NO concentrations of 7.1×10^{12} and 1.71×10^{14} cm^{-3} respectively. The converted OH signal is detected after 6.6 ms (time of detection). For the high conversion efficiency case, the contribution of RO_2 to the OH signal at 6.6 ms is about 35 % or 31 % of the initial RO_2 mixing ratio. This value matches with estimates from a previous study by Hens et al. (2014). For the low conversion efficiency case that represents the CYPHEX measurement mode, the estimated contribution of RO_2 to the measured signal is about 12 % or 2.5 % of the initial RO_2 mixing ratio.

Further, we estimate that more than 50 % of the RO_2 interference is due to isoprene oxidation products. This is due to the fast conversion of isoprene-based hydroxy peroxy radicals towards HO_2 and OH. These isoprene-based hydroxy peroxy radicals have one of the largest conversion efficiencies of up to 90 % (Fuchs et al., 2011; Lew et al., 2018). Moreover, we see that the RO_2 interference does not increase with increasing terpene concentrations and is nearly constant at terpene levels greater than 80 pptv (Fig. S2b), mostly because during the course of the day HO_2 concentration increases during this time faster than terpene-based RO_2 concentration. This indicates that the RO_2 interference effects cannot explain the deviation of modelled HO_2 with respect to measurements at high terpene mixing ratios (discussed later in Sect. 3.3 and 3.4).

Calibration of the instrument for OH and HO_2 measurements is achieved by measuring the signals generated by known amounts of OH and HO_2 (Martinez et al., 2010) in a calibrator set-up. The calibrator was mounted on top of the OH inlet without the IPI. Known amounts of OH and HO_2 were produced by irradiating different concentrations of humidified air with 185 nm radiation produced by a Pen-Ray Hg lamp. The actinic flux density of the Hg lamp (Pen-

Ray line source, LOT-Oriel, Germany) used for the photolytic radical production was determined before and after the campaign using the actinometry method by N_2O photolysis (Martinez et al., 2010). Different H_2O mixing ratios were produced by mixing different combinations of humidified and dry air flows using mass flow controllers. The humidified air was generated by bubbling dry air into a container half filled with water maintained at 25–30 °C. The water mixing ratio in the humid air stream was measured with a LI-COR CO_2/H_2O-analyzer (Li-7000) based on the detection of differential absorption with an infrared spectrometer. The stability of the Li-7000 was ensured by calibrations with a dew point generator (Li-610 from LI-COR).

The precision and minimum detection limit for OH measurements during CYPHEX were determined from the variability in the background signals (Table 1). The chemical background, during propane injection, being larger than the spectroscopic background (off resonance), has a dominating impact on the precision. The precision for OH and HO_2 measurements was calculated to be 4.8×10^5 molecules cm^{-3} and 0.39 pptv respectively for 4 min and 14 s time resolutions respectively. The accuracy for OH measurements was derived from the uncertainties in OH calibrations, which involve uncertainties in determination of lamp flux (traceable to a NIST NO standard), flows (calibrated with a DC-2B, traceable to IS0/RVA 17025), H_2O mixing ratios (calibrated with a Li-610), and uncertainties in estimation of OH losses in the IPI, accumulating to 28.5 % (2σ). The accuracy in HO_2 measurements was estimated to be 36 % (2σ) based on calibrations, loss of HO_2 in the IPI, and the uncertainty in NO mixing during titrations.

2.3 Measurements of other chemical and meteorological parameters

During CYPHEX, measurement instruments (Table 1) were set up in four air-conditioned laboratory containers, placed in two stacks of two. An 8 m tall, 0.5 m diameter, high-flow ($10\,m^3\,min^{-1}$) common inlet installed between the stacks was used to draw ambient air for most instruments. The references to the various measurements are indicated in Table 1. C_2-C_4 alkanes and alkenes (ethane: C_2H_6; ethene: C_2H_4; propane: C_3H_8; propene: C_3H_6; butane: C_4H_{10} (*i* and *n*); butene: C_4H_8 (*c* and *t*)) were measured with a time resolution of 60 min and the mixing ratio represents an average over a sampling period of 20 min (Sobanski et al., 2016). Photolysis frequencies were obtained with a charge-coupled device spectroradiometer (Metcon GmbH) operating at 275–640 nm with a 2-π integrating hemispheric quart dome. The spectroradiometer was calibrated prior to the campaign using a 1000 W NIST traceable irradiance standard. Photolysis frequencies were calculated using molecular parameters recommended by the International Union of Pure and Applied Chemistry (IUPAC) and NASA evaluation panels (S. P. Sander et al., 2011; IUPAC, 2015). An automatic weather station (Vantage Pro2; Davis Instruments Corp., Hayward, CA) was used to measure temperature, pressure, wind direction and speed, solar radiation, and humidity with a time resolution of 1 min.

2.4 The CAABA/MECCA model

Due to the high reactivity of OH with a plethora of anthropogenic and biogenic HCs, the HO_x chemistry of the atmosphere involves numerous reactions. To efficiently evaluate these reactions, several mechanisms of various complexity have been developed, e.g. the Regional Atmospheric Chemical Mechanism (RACM; Stockwell et al., 1997), the Master Chemical Mechanism (MCM; http://mcm.leeds.ac.uk, last access: 28 December 2017), the Mainz Isoprene Mechanism (MIM; Taraborrelli et al., 2009), the Carbon Bond Mechanism (Yarwood et al., 2005). For this study, we use the Module Efficiently Calculating the Chemistry of the Atmosphere (MECCA; S. P. Sander et al., 2011; R. Sander et al., 2005), which is an atmospheric chemistry module that contains a comprehensive set of gas- and aqueous-phase chemical reaction mechanisms covering tropospheric and stratospheric chemistry. The gas-phase chemistry in the present version contains 2664 species (including 40 dummy species to account for deposition) and 1670 reactions, including basic O_3, CH_4, HO_x, NO_x, non-methane hydrocarbon (NMHC), and sulfur chemistry. Complex organic chemistry is taken from the Mainz Organic Mechanism (MOM; Taraborrelli et al., 2015). MOM is based upon MIM3, containing new additions to an isoprene oxidation mechanism (MIM2) for regional and global atmospheric modelling. Under pristine conditions, isoprene oxidation buffers OH to a narrow range of concentrations (Taraborrelli et al., 2009).

The original MIM is based on MCM. MIM2 was further developed to improve the tropospheric chemistry under a wide range of NO_x regimes and provided a better evaluation of NO_x and organic nitrogen-containing species due to a detailed representation of the alkyl and peroxy acyl nitrates as well as isoprene oxidation products, some of which can be measured using modern instrumentation, e.g. methyl vinyl ketone (MVK), methacrolein (MACR), hydroxyacetone, and methyl glyoxal (Taraborrelli et al., 2009). MIM3 is a reduced version of MIM2, suitable for 3-D atmospheric chemistry-transport modelling. It contains an improved isoprene oxidation mechanism related to OH recycling. It accounts for the photo-oxidation of unsaturated hydroperoxy aldehydes, a product of isoprene oxidation, initiating a hydroxyl radical production cascade. Compared to RACM, MIM3 presents a lower degree of lumping and reproduces the mixing ratios of the main chemical species in the atmosphere and many intermediates very well under a tropical mid-NO_x scenario (Taraborrelli et al., 2012). In MIM3, the extended chemistry following the OH and O_3 pathways has been thoroughly revised, tested in a box model, and shown to reproduce HO_x measurements, even for challenging conditions

Table 1. Details of experiments conducted during CYPHEX (relevant to this study). PTR-TOF-MS: proton-transfer-reaction time-of-flight mass spectrometry. GC-FID: gas chromatography–flame ionization detector.

Species	Measurement technique	Time resolution	Precision	Limit of detection	Total uncertainty	Reference
Hydroxyl radical	LIF-FAGE-IPI	4 min	4.8×10^5 molec cm^{-3}	1×10^6 molec cm^{-3}	28.5 % (2σ)	Hens et al. (2014)
Hydroperoxyl radical	LIF-FAGE	14 s	0.4 pptv	0.8 pptv	36 % (2σ)	Martinez et al. (2010)
Ozone	UV photometry	1 min		2 ppbv	5 %	Li et al. (2015) Hosaynali Beygi et al. (2011)
Carbon monoxide	Room temperature Quantum cascade Laser spectrometer	1 s		0.4 ppbv	14.4 %	Li et al. (2015)
Nitric oxide Nitrogen dioxide	Chemiluminescence	5 s		5 pptv 20 pptv	20 % 30 %	Li et al. (2015) Hosaynali Beygi et al. (2011)
Nitrous acid	Long-path absorption photometry	30 s		4 pptv	10 %	Meusel et al. (2016)
Formaldehyde	Hantzsch reaction fluorescence	10 min		38 pptv	16 %	Kormann et al. (2003)
Hydrogen peroxide Organic peroxides	Enzymatic reaction	10 min		14.9 pptv	16 % 20 %	Fischer et al. (2015)
Methyl hydroperoxide	High-performance liquid chromatography	12 min	3 %	25 pptv	9 %	This study
SO_2	Chemical ionization mass spectrometer	10 mins		50 pptv	30 %	
C_2-C_4 (alkanes, alkenes)	GC-FID	60 min	< 5 %	1–8 pptv	10 %	Sobanski et al. (2016)
Methane	GC-FID	1 min	2 %	20 ppbv	2 %	This Study
Isoprene α-pinene β-pinene Limonene	GC-MS	45 min	3.3 % 4.9 % 8.8 % 4.2 %	1 ppt 1 ppt 2 ppt 1 ppt	14.5 % 15 % 16.7 % 14.7 %	Derstroff et al. (2017)
	PTR-TOF-MS	1 min	1σ	3σ	1σ	Derstroff et al. (2017)
Benzene			5.4 % (at ∼ 280 pptv)	14 pptv	14 % (21 %*)	
Toluene			4.9 % (at ∼ 280 pptv)	12 pptv	14 % (20 %*)	
Isoprene oxid. pdts.			5.0 % (at ∼ 260 pptv)	14 pptv	11 % (14 %*)	
Methyl ethyl ketone (MEK)			3.8 % (at ∼ 280 pptv)	16 pptv	11 % (16 %*)	
Methanol			2.5 % (at ∼ 2800 pptv)	242 pptv	37 % (41 %*)	
Acetaldehyde			2.2 % (at ∼ 1300 pptv)	85 pptv	22 % (27 %*)	
Acetone			1.4 % (at ∼ 2500 pptv)	97 pptv	10 % (17 %*)	
Acetic acid			9.2 % (at ∼ 900 pptv)	264 pptv	51 %	

* Total uncertainty for the lower humidity range (< ca. 25 % relative humidity).

with high isoprene mixing ratios (< 1 nmol mol^{-1}) and low NO (< 40 pmol mol^{-1}) (Taraborrelli et al., 2012).

MOM was first presented and used in the study by Lelieveld et al. (2016). It represents the gas-phase oxidation of more than 40 primarily emitted VOCs. The structure and the construction methodology mirrors that of the MCM. The oxidation mechanism for aromatics has been presented in Cabrera-Perez et al. (2016). The terpene oxidation scheme includes previous developments for modelling HO_x field measurements (Taraborrelli et al., 2012; Hens et al., 2014; Nolscher et al., 2014). Most of the known and/or proposed HO_x-recycling mechanisms under low-NO conditions are taken into account. Finally, isoprene chemistry follows, to a large extent, Peeters et al. (2014) and Jenkin et al. (2015), with modifications by Nolscher et al. (2014). Chemistry of the pinenes (monoterpenes) is a reduction of the MCM with modifications proposed in the past by Vereecken et al. (2007), Nguyen et al. (2009), Vereecken and Peeters (2012), and Capouet et al. (2008). For the numerical integration, MECCA uses the KPP software (Sandu and Sander, 2006). All gas-phase reactions are contained in a single chemical file (gas.eqn).

The most common method to efficiently evaluate a complex chemical environment is to use a zero-dimensional, photochemical box model. Here, we use version 3.8 of the box model CAABA (Chemistry As A Boxmodel Application),

Table 2. Deposition velocities of some important species considered in the model scheme.

Species	Deposition velocity ($cm\,s^{-1}$)
Peroxides	4
PAN	0.2
NO_3	4
HNO_3	4
PINAL	0.6
HCOOH	1

which is based on version 3.0 described by R. Sander et al. (2011). To apply the MECCA chemistry to atmospheric conditions, it is connected to the CAABA base model via the MESSy interface. The model is constrained by observed concentrations of the main reactive trace gases, O_3, CO, NO, NO_2, nitrous acid (HONO), HCHO, hydrogen peroxide (H_2O_2), methyl hydroperoxide (MHP, CH_3OOH), SO_2, C_2-C_4 alkanes and alkenes, isoprene, pinene (α and β), limonene, benzene, toluene, methane, methanol, acetonitrile, acetaldehyde, acetone, acetic acid, and photolysis rate constants. Model results were obtained by letting the model run into steady state for OH and HO_2 for each set of data points. The steady state was set to be achieved for OH when the relative changes in OH were less than 5×10^{-7}. Deposition velocities used in our scheme for some important species are provided in Table 2. The deposition is incorporated into the model scheme by converting a species into a dummy species according to its deposition velocity. As these dummy species will not participate in any further chemical reaction, their precursors are effectively removed from the model chemical scheme. The deposition velocities of peroxides and formic and nitric acid are based on Nguyen et al. (2015) while those for PINAL and PAN are based on Evans et al. (2000), using the average of the deposition rates for water, forest, and grass. The model scheme is included in the Supplement.

2.5 The FLEXPART model

In order to understand the impact of different emission sources on the atmospheric processing of air masses, the dynamical transport history of air parcels reaching Cyprus during the CYPHEX campaign was traced using FLEXPART 9.2 (Stohl et al., 2005). FLEXPART is a Lagrangian particle dispersion model that describes the transport and diffusion of tracers by computing the trajectories of a large number (ca. 10 000) of infinitesimally small tracer particles. For CYPHEX, trajectory simulations were performed at 3 h time intervals during 21–31 July 2014. For this, FLEXPART was run 120 h backward in time from the measurement site driven with analyses from ECMWF with $0.2° \times 0.2°$ horizontal resolution and a temporal resolution of 1 h (Hüser et al., 2017). The particle density distribution of the tracer particles during this 12 h backward simulation provided information on their residence time in each grid cell of the defined geographical area (Fig. S3). Major transport routes of air reaching the site during CYPHEX were identified from the grid cells with higher residence times.

3 Results and discussion

3.1 HO_x measurements during CYPHEX and associated meteorological and chemical parameters

The variation in OH and HO_2 along with a few important chemical and radiation parameters relevant to HO_x chemistry during 21–31 July (day of the year: 202–212) are shown in Fig. 2. The mean values of OH and HO_2 during 21–31 July were 2.2×10^6 and 2.87×10^8 molecules per cm^3 respectively. The mean OH concentration during peak noon hours ($J(O^1D) > 2 \times 10^{-5}\ s^{-1}$) was 5.75×10^6 molecules per cm^3. While both OH and HO_2 showed a clear diurnal variation, the HO_2 / OH ratio decreased with enhancement in $J(O^1D)$, and was close to 100 at $J(O^1D) = 3 \times 10^{-5}\ s^{-1}$. During the MINOS campaign in the summer of 2001 on Crete, an island in the central Mediterranean at similar latitude about 700 km west of the CYPHEX site, average OH levels were measured to be $3.6 - 6.7 \times 10^6$ molecules per cm^3 (Berresheim et al., 2003). The peak OH levels during MINOS reached twice the peak values observed during our study on Cyprus. During MINOS, OH peaked at about 2.1×10^7 molecules per cm^3, with O_3 and $J(O^1D)$ of about 60 ppbv and $2.8 \times 10^{-5}\ s^{-1}$. These O_3 and $J(O^1D)$ values are not very different from CYPHEX values, indicating that the peak primary OH production would not be very different for MINOS and Cyprus. Although HO_2 was not measured during MINOS, the CO levels (mean values reaching close to 160 ppbv) were much higher (Heland et al., 2003) compared to CYPHEX, indicating the possibility of higher HO_2. Nevertheless, the absence of HO_2 measurements during MINOS impairs our ability to directly compare the OH chemistry from the two datasets for a regional perspective. However, the peak OH levels observed during CYPHEX are comparable to the midday OH concentrations predicted for the Finokalia Aerosol Measurement Experiments (FAME-08) at a remote coastal site on the island of Crete, Greece (Hildebrandt et al., 2010). The FAME measurements showed the presence of aged, highly oxygenated organic aerosols (OAs) during summer compared to winter despite being heavily influenced by continental air masses (53 %) during summer and aged marine air masses (61 %) during winter. The presence of highly oxygenated OA during summer was attributed to strong photochemical impacts due to higher O_3 and UV levels during summer, leading to double the values of midday OH concentrations during summer compared to winter (Hildebrandt et al., 2010).

While OH measurements during CYPHEX started on 12 July 2014 (day of year: 193), systematic HO_2 measure-

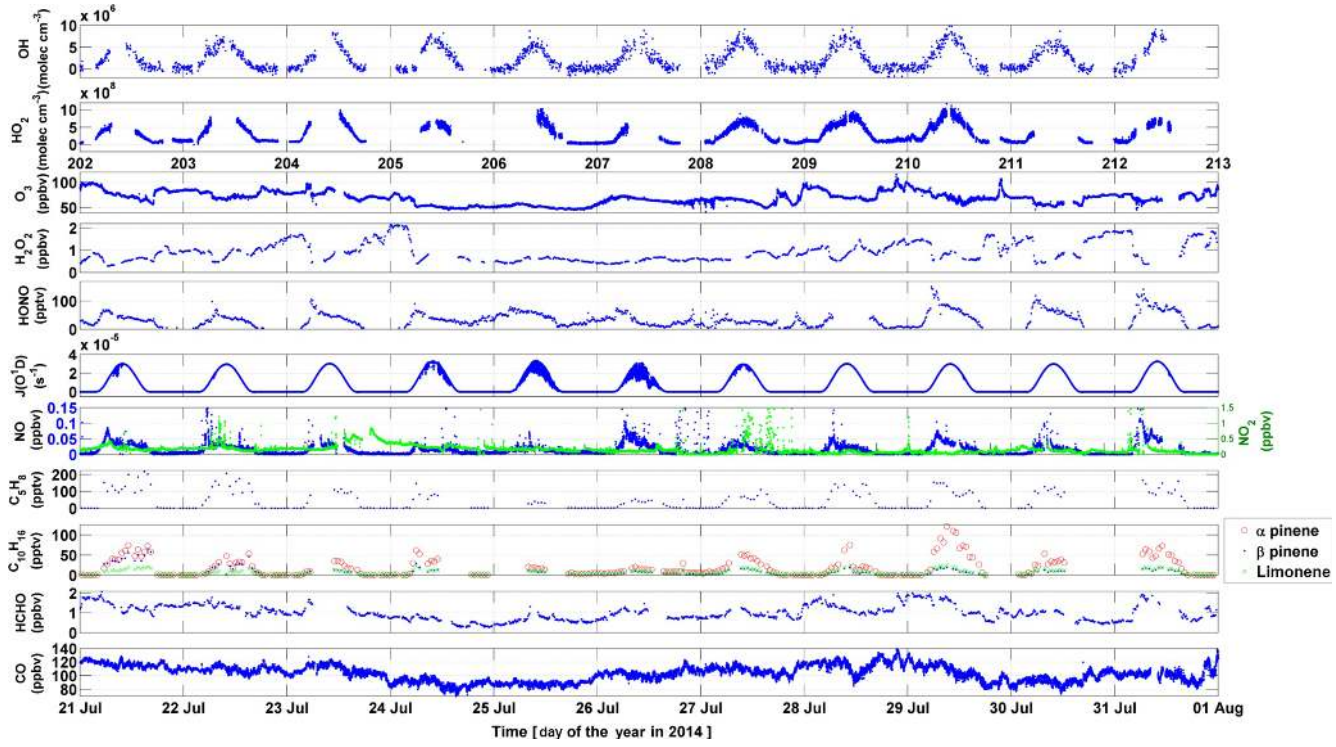

Figure 2. Measurements of OH, HO_2, and selected chemical and radiation parameters relevant to HO_x chemistry during the CYPHEX campaign. Time is in UTC. Local time in Cyprus during summer is UTC+3.

ments started much later from 21 July 2014 (day of year: 202). Simultaneous measurements of OH and HO_2 during CYPHEX are available for the period 21–31 July, and the discussion in this work is based on this common dataset. Large day-to-day changes in concentrations of several OH and HO_2 precursors were observed during the study period; e.g. O_3 varied from 50 to 110 ppbv, CO from 70 to 140 ppbv, and HCHO from 0.2 to 2 ppbv. The noontime OH and HO_2 levels were 5.75×10^6 (± 43 %) and 6.25×10^8 (± 30 %) molecules per cm^{-3} respectively (Fig. 2). While the average concentrations of O_3 and CO during the study period (days of year: 202–212) were 69 and 104 ppbv respectively during days 205 and 206, the mean O_3 and CO values were 22 % and 33 % lower. The later period, i.e. days 205 and 206, correspond to air masses arriving from southwestern Europe and passing over the Mediterranean with predominantly marine influence (reaching over 70 % for 5-day simulations using FLEXPART). The large changes in O_3 and CO under different air mass regimes do not translate into the changes in HO_x levels (Fig. 2). This is because their concentrations are to some extent buffered as sources and sinks tend to increase in parallel in relation to anthropogenic and biogenic emissions. To study the impact of these numerous reactions on the HO_x budget, we used a photochemical box model (CAABA/MECCA).

3.2 Modelling simulations of CYPHEX HO_x

Figure 3 shows simulations of OH and HO_2 using CAABA/MECCA in comparison with the measurements in ambient air. Due to the remote location of the measurement site, it is expected that the HO_x chemistry would be representative for the background Mediterranean atmosphere. In general, NO levels were low during CYPHEX, with only ~ 2 % of data above 1 ppbv NO and ~ 5 % above 100 pptv of NO. The study is limited to NO below 100 pptv to exclude measurements affected by emissions from the local diesel generator and local automobile traffic. Under very remote conditions, the steady state of HO_x would be achieved from a balance between HO_x production (Reactions R1–R3) and HO_x loss (Reaction R10). However, such a simplified condition is rarely achieved in the boundary layer as the presence of HCs leads to additional production and loss channels. A first model run was carried out constraining only O_3, CO, CH_4, NO, NO_2, HONO, HCHO and H_2O_2, H_2O, and photolysis frequencies to measured values (Fig. 3, case I). Thus, the major primary production channels for OH and HO_2 via photolysis of O_3, HONO, and HCHO are constrained by measured quantities, while the recycling of OH and HO_2 occurs via reactions with O_3, CO, CH_4, and NO only. However, in the absence of the contribution from important HCs, OH loss is underestimated, leading to an over-prediction of OH on the order of 88 %. Further, HO_2 is also overestimated, on aver-

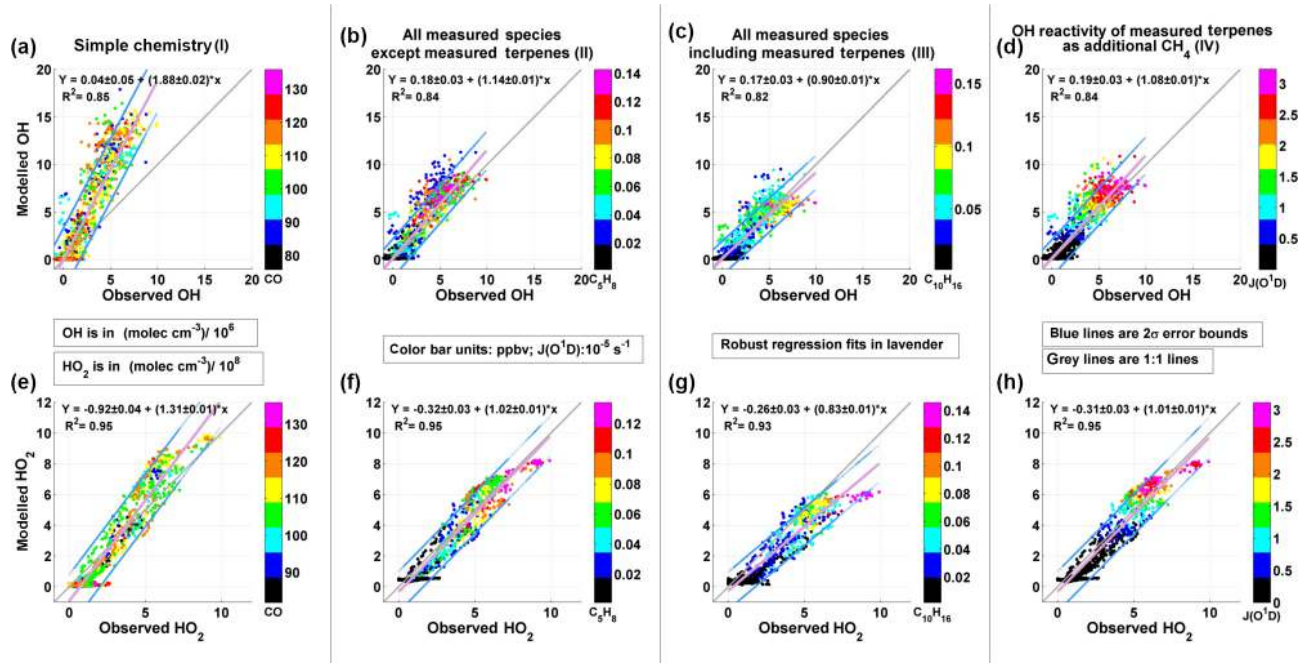

Figure 3. LIF-FAGE measurements of OH **(a–d)** and HO_2 **(e–h)** vs. model simulations with CAABA/MECCA. From left to right: model simulations using simple chemistry without NMHCs (case I), simulations including anthropogenic and biogenic hydrocarbons except terpenes (case II), after adding terpenes (case III), and after initializing with zero terpenes but with CH_4 increased to account for the additional measured terpene reactivity (case IV).

age, by more than 30 % in this case (Fig. 3, case I) as loss via formation of hydroperoxides is under-represented due to the incomplete VOC representation, leading to too low RO_2 concentrations.

When we constrain the model with all measured species, the OH simulations are much improved with a model-to-measured ratio of 0.90 (Fig. 3 case III). However, HO_2 is now under-predicted by about 17 %. The under-prediction of HO_2 is enhanced with increasing terpene (α-pinene, β-pinene, and limonene) mixing ratios, with an average HO_2 model / measurement ratio of 0.72 for > 80 pptv of measured terpenes. When terpenes are not included in the model, the HO_2 simulations are much improved (model / measured = 1.02). The mean daytime OH reactivity calculated for the measured major terpenes was about $0.06\,s^{-1}$. This value is only 3.7 % of the calculated reactivity from the total of all measured species and about 10.7 % of the OH reactivity (k_{OH}; Eq. 1) from CO. The OH reactivity calculated from the trace gases measured during CYPHEX varied between 1 and $2\,s^{-1}$ during the study period (Fig. 4), which is comparable to reactivity measurements made in the free troposphere (Mao et al., 2009). During the TORCH-2 campaign in Weybourne, England, and the DOMINO campaign in El Arenosillo, Spain, the total reactivity was generally $< 5\,s^{-1}$ when air masses originated from the sea (Lee et al., 2009; Sinha et al., 2012). The OH reactivity measured in suburban regions is generally higher than $5\,s^{-1}$ (Yang et al., 2016). During CYPHEX, CO and CH_4 constituted more than half of the total calculated reactivity (Fig. 4). CO, CH_4, HCHO, C_5H_8, and CH_3CHO accounted for 35 %, 17 %, 13 %, 9 %, and 8 % respectively of the calculated OH reactivity for daytime values during CYPHEX.

$$k_{OH} = \sum (k_{species} \times C_{species}), \quad (1)$$

where $k_{species}$ is the rate coefficient for reaction of a given species with OH and $C_{species}$ is the concentration of the same species.

As limonene chemistry is not included in the current model scheme, it is accounted for in the model in the form of additional α-pinene after normalizing for their OH reactivities. When limonene is included as CH_4 instead of α-pinene, the OH loss increases by about 1 % compared to case II in which there were no terpenes in the model, which confirms the average OH reactivity of limonene at $0.02\,s^{-1}$, i.e. an additional 1 % of the calculated reactivity from the measured species. Although limonene chemistry is different from α-pinene in that it caters more towards secondary organic aerosol (SOA) formation, addition of limonene as α-pinene increases HO_2 and OH losses by 3 %–6 %, which is well within the uncertainty of the measurements. Nevertheless, the degradation products from terpene oxidation (shown in Fig. 5) further act as sources and sinks for OH and HO_2, hence playing an important role in the overall HO_x chemistry (Calogirou et al., 1999; Librando and Tringali, 2005;

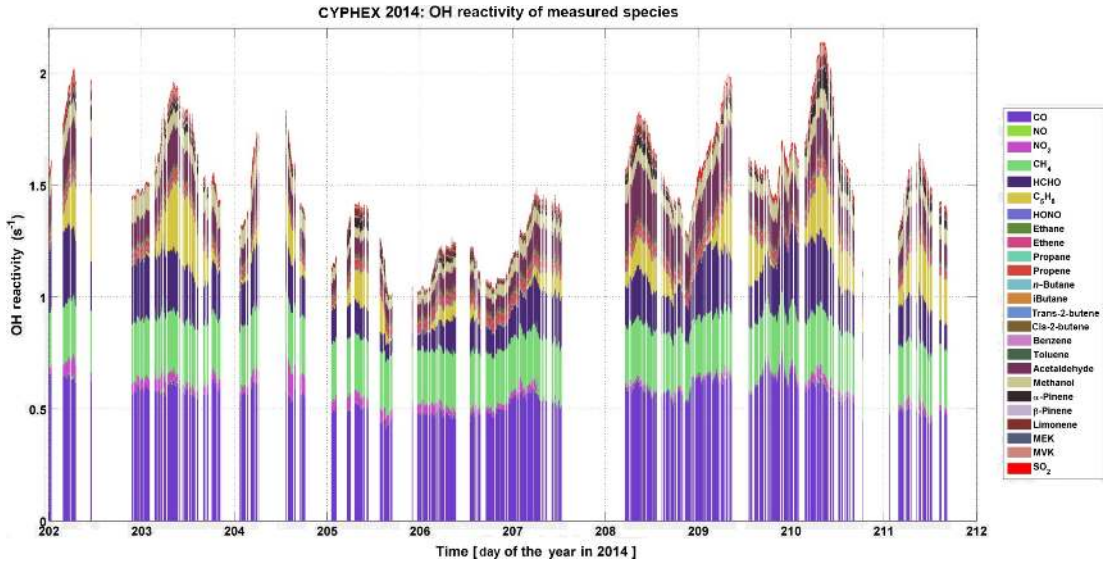

Figure 4. Calculated OH reactivity of various chemical species measured during CYPHEX.

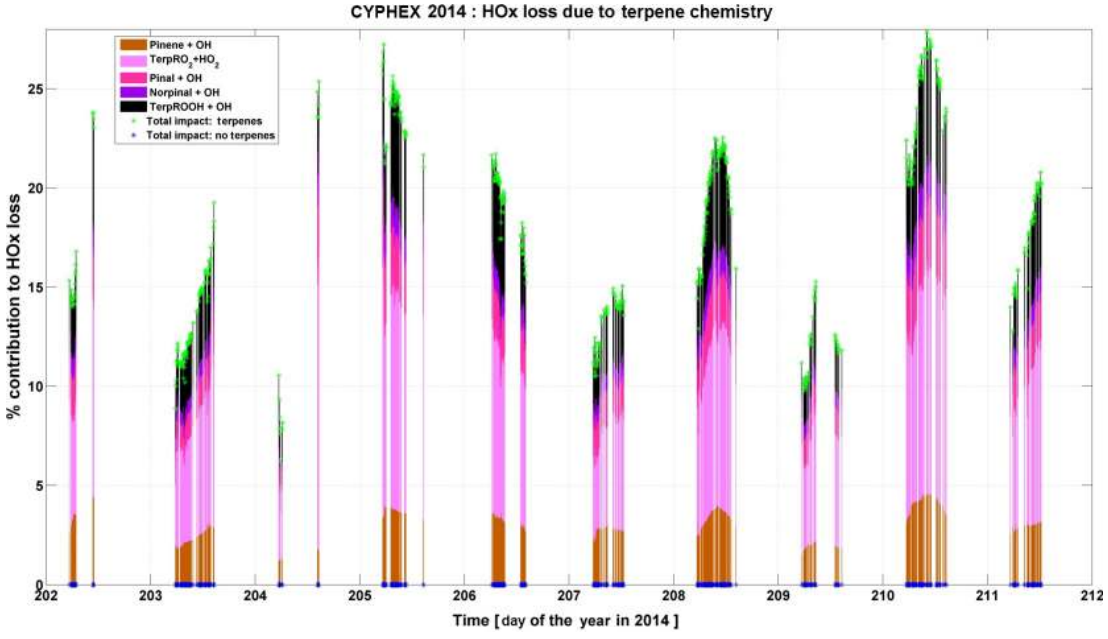

Figure 5. Contribution of different terpene-related reactions to the total HO_x loss. Additional peroxy radicals are produced in the model by terpenes rather than organics, e.g. isoprene degradation. Pinene includes α-pinene and β-pinene. TerpRO2 includes only $C_8H_{13}O_3$ (C85O2), $C_8H_{13}O_4$ (C86O2), $C_9H_{15}O_3$ (C96O2), $C_9H_{15}O_4$ (C97O2), $C_9H_{15}O_5$ (C98O2), $C_{10}H_{15}O_5$ (C106O2), $C_5H_7O_4$ (C511O2), $C_6H_9O_5$ (C614O2), $C_{10}H_{15}O_4$ (PinalO2), and $C_{10}H_{17}O_3$ (BPinaO2). TerpROOH includes only $C_{10}H_{16}O_4$ (PinalOOH), $C_8H_{14}O_3$ (C85OOH), $C_8H_{14}O_4$ (C86OOH), $C_9H_{16}O_4$ (C97OOH), $C_9H_{16}O_5$ (C98OOH), $C_{10}H_{16}O_5$ (C106OOH), and $C_5H_8O_4$ (C511OOH). The names in brackets are MCM nomenclature. Only those species are selected whose contribution is at least 0.25 % to the HO_x sink.

Zhang et al., 2015; Wisthaler et al., 2001). Further, increasing or decreasing the terpene concentrations by their measured uncertainties (15 %; Table 1) decreases or increases the OH and HO_2 model / measured slope by 2 %–3 %, which is close to the errors on the regression slopes. Also, changing other gases like CO and C_5H_8 by their uncertainties (Table 1) has less than 3 % impact on the model vs. measured slopes for OH and HO_2. Nevertheless, when terpenes are included as CH_4, both OH and HO_2 simulations are much improved (Fig. 3, case IV). In this case, the terpene chemistry does not play any role in OH–HO_2 simulations but the primary OH reactivity of terpenes is taken into account.

To access the model uncertainty, Monte Carlo simulations are carried out by selecting 228 data points from the input dataset, representing at least two occurrences of concentrations, i.e. 1–15, 25–75, and 85–99 percentiles of O_3, CO, NO, HCHO, HONO, C_5H_8, $C_{10}H_{16}$, and $J(O^1D)$. For each of these points, we performed 9999 Monte Carlo simulation runs. The Monte Carlo simulations are based on the method described in R. Sander et al. (2011), but additionally we varied the boundary conditions of the measured species by their $\pm 1\sigma$ uncertainty (Table 1). The derived overall model uncertainty at 1σ is 17.4 % and 10.5 % for OH and HO_2 respectively.

Review studies show agreements between in situ observations of OH and HO_2 and box model calculations using different chemical schemes within a factor of 2 for both urban and marine (boundary layer) environments (Stone et al., 2012). During the North Atlantic Marine Boundary Layer Experiment (NAMBLEX) field campaign in the summer of 2002 at the Mace Head Atmospheric Research Station, OH was under-predicted early in the morning and in the late afternoon–early evening and over-predicted in the middle of the day based on simple steady-state calculations (Smith et al., 2006). However, photolysis of HONO was not considered due to the absence of HONO measurements during NAMBLEX. The authors contemplate that HONO photolysis and OH recycling could play crucial roles in explaining the discrepancy between measured and calculated OH during periods with a high solar zenith angle. Despite low-isoprene regimes (Lewis et al., 2005), inclusion of dimethyl sulfide (DMS) and C_5H_8 improved the calculated / measured ratio for OH from 1.13 ± 0.36 to $0.94 + 0.39$ during NAMBLEX. HO_2 was over-predicted but model performance improved by incorporating reactions with BrO, IO, and aerosol uptake; the best-case scenario for HO_2 modelled / measured was 1.26 ± 0.36. During the Intercontinental Chemical Transport Experiment-A (INTEX-A), OH was predicted fairly well for the lowest 2 km over North America and the western Atlantic Ocean using a zero-dimensional, time-dependent photochemical box model developed at NASA Langley Research Center (Ren et al., 2008). In the study, HO_2 was over-predicted (model / measurement = 1.37). It is challenging to put the model–measurement agreement during CYPHEX in perspective with other studies because they vary with respect to chemical regimes, i.e. different amounts of NO_x and HCs as well as the chemical mechanisms employed to simulate the HO_x chemistry. Rohrer et al. (2014) compared the HO_x chemistry from different field campaigns using a common modelling framework and point to buffering mechanisms that maintain OH in various NO_x and VOC regimes. Ren et al. (2008) have noted that despite highly constrained measurement suites during various field campaigns, there are significant discrepancies between model predictions and actual measurements of OH and HO_2 in different environments. One possible reason for the discrepancy could be due to unmeasured atmospheric constituents. However, during CYPHEX we have been able to measure the major primary sources and sinks related to HO_x chemistry, and simulations agree within uncertainty of OH and HO_2 measurements. Another plausible reason for discrepancy is the uncertainty in mechanistic pathways, branching ratios, and rate constants, etc., which are not known with sufficient accuracy. A recent study comparing seven different chemical mechanisms constrained with the same input data and boundary conditions revealed 25 %–40 % ambiguity in predictions of HO_2 and OH over the United States (Knote et al., 2015). As we highlight in the next section, the HO_x chemistry related to terpenes is also associated with substantial uncertainty.

3.3 Reasons for decreased model accuracy when including the terpene chemistry

As discussed in the last section, we find that the under-prediction in HO_2 gradually increases with increasing terpene levels, being about 38 % for the highest terpene levels observed (about 120 pptv). To ascertain if this under-prediction is related to terpene chemistry or some other chemical pathway, we compare two model runs, namely case III vs. case IV in Fig. 3. Case IV is achieved by initializing the model with zero terpenes, however keeping the terpene reactivity towards OH intact. The terpene reactivity, i.e. the product of individual terpene concentrations with their rate coefficient towards OH, is approximated in the model scheme in the form of additional CH_4 (Fig. 3, case IV). Under this scenario, we find that the agreement between modelled and observed HO_2 again improves, to levels similar to case II without terpenes in the model (Fig. 3). The small difference of 6 % with respect to OH prediction between cases II and IV (Fig. 3) also corroborates the minor primary reactivity of $< 0.06\,s^{-1}$ for the sum of α-pinene, β-pinene, and limonene towards OH. However, up to 38 % under-prediction in HO_2 for terpene concentrations over 80 pptv indicates the important role of secondary products formed during terpene oxidation in the HO_x budget.

To quantify the magnitude of the impact of terpene degradation products on the HO_x budget, we compared the HO_x sinks from the two model cases: case III (Fig. 3, henceforth "terpene case") and case II (Fig. 3, henceforth "isoprene case"), the difference being the presence and absence of α-pinene, β-pinene, and limonene. The estimation of HO_x sinks from the two model cases is conspicuously marked by significant contribution of terpene degradation and oxidation products in the terpene case which are absent in the isoprene case. The additional reactions in the terpene case make up 6.3 %–27.8 % of the total HO_x sinks, the contributions increasing with the terpene concentrations and peaking between 13:00 and 14:00 LT on clear days (Fig. 5). While the terpene degradation products contribute, on average, 15 % to the total HO_x loss, this value is 20.5 % for terpenes > 80 pptv. The corresponding contribution of terpene-related peroxy radicals to the total HO_x loss is 7.8 % and

10.3 % respectively, accounting for about 52 % of the impact of the terpene degradation products, including peroxy radicals, pinal, norpinal, and peroxides, towards HO_x loss.

Since only about 3.7 % of primary terpene reactivity with OH results in up to 28 % of HO_x loss, with terpene-generated peroxy radicals having more than 4 times the impact of the primary terpenes on the HO_x loss, we examine a sequence of reactions starting with the oxidation of α-pinene to understand the genesis and propagation of these terpene-generated peroxy radicals (Reactions R15–R23). The reactions show that oxidation of α-pinene via OH and O_3 directly generates several peroxy radicals (Reactions R15–R16), which are sinks for HO_x via their reactions with HO_2-forming hydroperoxides (e.g. Reactions R21–R22). These first-generation peroxy radicals also form other peroxy radicals (Reactions R17–R20), and the chain propagates to produce additional peroxy radicals contributing via formation of the respective hydroperoxide in reaction with HO_2, leading to overall HO_x loss (e.g. Reaction R23).

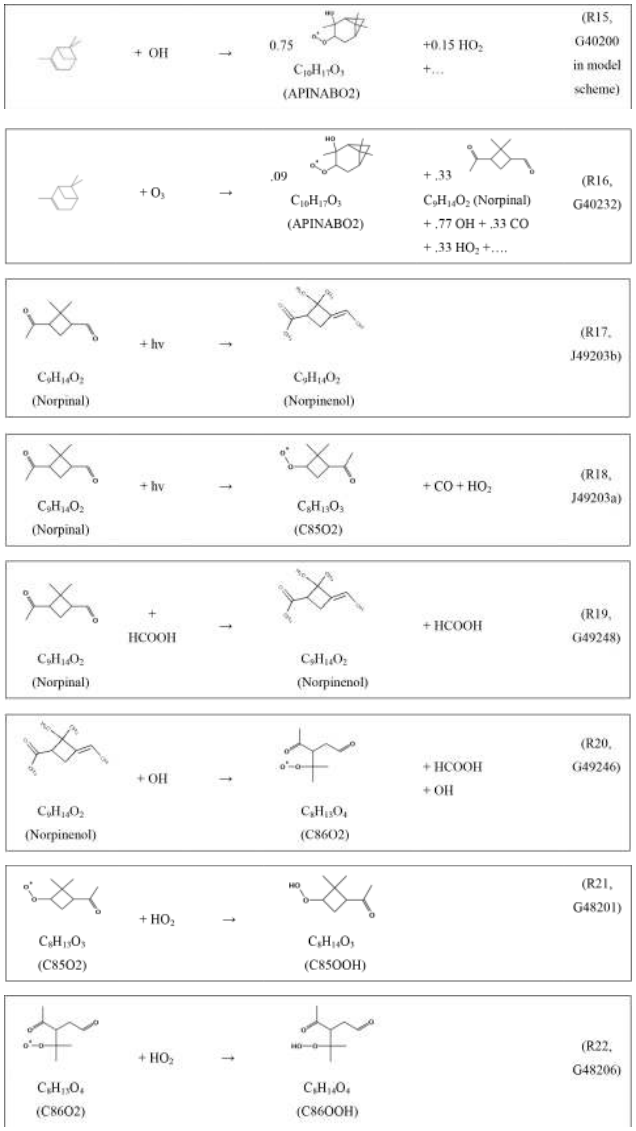

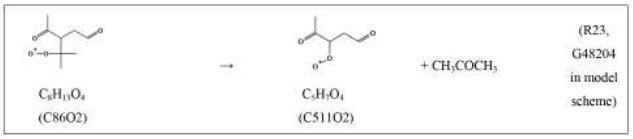

Thus, a cascade of HO_x scavengers mostly in the form of RO_2 species, at low NO_x levels, starting with oxidation of primary terpenes, leads to nearly 28 % HO_x loss, resulting in up to 38 % under-prediction of HO_2. The losses increase with increases in terpene levels. The major contribution towards the HO_x loss comes from terpene-generated organic peroxy radicals (Fig. 5). However, there are major uncertainties regarding the chemical pathways and rate coefficients governing the chemistry of these peroxy radicals in the actual atmosphere and in the next section we examine several postulates based on the literature.

3.4 Terpene-generated organic peroxy radicals

A limitation in our understanding of peroxy radical oxidation pathways is the rate constant of peroxy radicals with NO. For most peroxy radicals, lumped rate coefficients are defined by the expression Eq. (2) (Rickard and Pascoe, 2009) as kinetic data are unavailable for most of the RO_2–NO reactions.

$$K_{RO_2NO} = 2.54 \times 10^{-12} \exp(360/T).f \quad (2)$$

Thus, K_{RO_2NO} is the product of the rate coefficient and an efficiency factor, f. The values of f for different classes of RO_2 are given in Jenkin et al. (1997). The reaction of RO_2 with NO can proceed via two channels, one forming alkyl nitrate ($RONO_2$) and the other forming RO and NO_2 (Reactions R12–R13). Enhancing the RO_2–NO rate coefficient suppresses the peroxide-forming channel via HO_2. For our study period, increasing the K_{RO_2NO} even by a factor of 4 led to only a 6.8 % increase in modelled HO_2 levels for terpenes > 80 pptv (Fig. 6).

During the summertime 1999 Southern Oxidants Study (SOS) at Nashville, Tennessee, agreement could be found between photochemical models and in situ measurements when the product of the branching ratio and rate constant for organic peroxide formation, via Reaction (R11), was reduced by a factor of 3–12 (Thornton et al., 2002). To test this hypothesis, we decreased the $K_{RO_2HO_2}$ for terpenes by half and by one-fifth of its value considered in the model. The rate coefficient of RO_2 with HO_2 leading to ROOH is given by Eq. (3), where $K_{RO_2HO_2}$ increases with the size of RO_2 radicals (Atkinson et al., 1999; Boyd et al., 1996) (http://mcm.leeds.ac.uk/MCMv3.3.1/categories/saunders-2003-4_6_4-gen-master.htt?rxnId=6942, last access: 28 December 2017).

$$K_{RO_2HO_2} = 2.91 \times 10^{-13} \exp(1300/T) \left[1 - \exp(-0.245n)\right], \quad (3)$$

where n is the carbon number and T is the temperature.

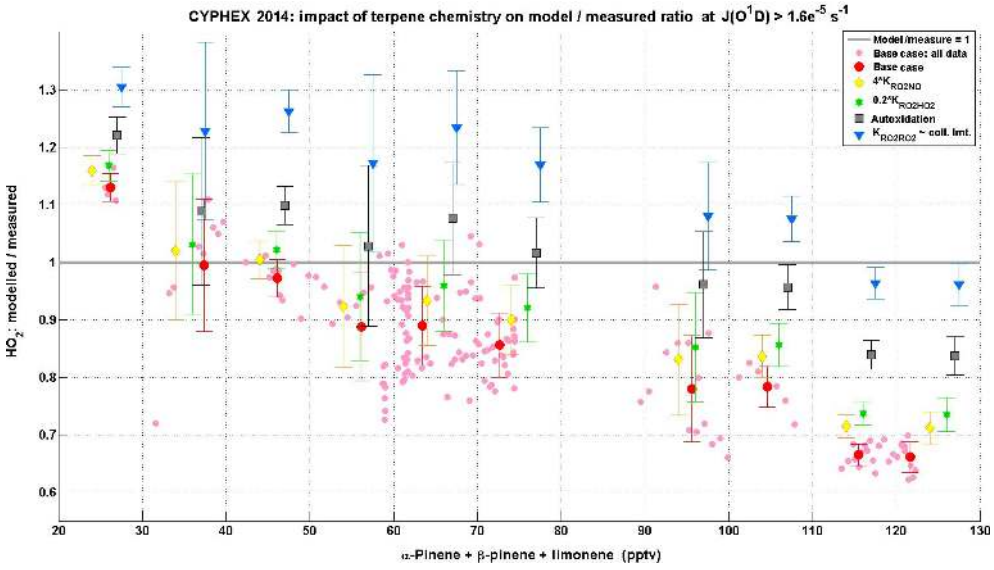

Figure 6. HO_2 predictions using different chemical schemes which were employed to investigate the impact of peroxy radicals as a HO_2 sink. The x axis shows the sum of measured α-pinene, β-pinene, and limonene. The base case is the model simulation using measured species; $4 \times K_{RO_2NO}$ is a simulation in which the rates of selected terpene-related RO_2 species with NO are increased by a factor of 4; $0.2 \times K_{RO_2HO_2}$ is a simulation in which the rates of these RO_2 species with HO_2 are reduced by a factor of 0.2; the autoxidation simulation includes an autoxidation scheme rapidly converting selected RO_2 species into ROOH. The last scheme refers to a simulation in which $K_{RO_2R'O_2}$ is set to 4×10^{-10} cm^3 molecule^{-1} s^{-1} (close to the collision limit). The mean and sigma are calculated for 100 pptv bins along the x axis.

We find that decreasing the rate coefficient by a factor of 5 leads to better reconciliation with our observations than when decreasing it by a factor of 2. When $K_{RO_2HO_2}$ was reduced by a factor of 5, the modelled HO_2 increased by only 9.9 % for higher terpene levels, i.e. α-pinene + β-pinene + limonene > 80 pptv (Fig. 6).

Recent studies have proposed inter- and intra-molecular hydrogen abstraction by peroxy radicals (autoxidation) to be effective reaction pathways leading to OH formation (Crounse et al., 2013). This abstraction is largely determined by the thermochemistry of the nascent alkyl radicals and thus is strongly influenced by neighbouring substituents; hence the rate increases rapidly when more oxygen-containing functional groups are involved. The H-shift rates reported in literature can be as fast as 0.1 s^{-1} for atmospheric conditions. We incorporated a simple autoxidation scheme for some of the most important terpene-related RO_2 species as specified in Fig. 5 in our model. In this scheme, the specific terpene-generated RO_2 species whose contribution was at least 0.25 % to the HO_x sink are converted into a corresponding ROOH at a very fast rate ($1e^{10} \times K_{RO_2HO_2}$), reaching up to 0.2 s^{-1}; e.g. $C_{10}H_{15}O_4$ (PINALO2) is converted to $C_{10}H_{16}O_4$ (PINALOOH). We find that this scheme is effective in increasing the model HO_2 levels by 24.2 % for terpene levels > 80 pptv (Fig. 6). Since we have used a very simple approach to test the impact of autoxidation in the model atmosphere, more studies are required for a mechanistic development for incorporating these schemes, namely which way the H shift will occur at which rate, which products will be formed, etc. The present exercise in implementing the autoxidation scheme is only meant to show its importance, effectiveness, and potential in atmospheric chemistry models.

Further, when we greatly increased the RO_2–$R'O_2$ reaction rates to 4×10^{-10} cm^3 molecule^{-1} s^{-1} (close to the collision limit), we found that the discrepancy of the modelled HO_2 loss with respect to the measurements with increasing terpenes decreases (Fig. 6) and the overall agreement between modelled and measured HO_2 is still good (Figs. 6, S4, and S5). The large deviation between observations and modelled HO_2 around midday on days 205, 208, and 210 occurs during periods with high terpene concentrations. On days 205 and 208, the simulation with the autoxidation scheme shows much better agreement with observations compared to the base case (Case III in Fig. 3) while on day 210, when terpene concentrations are much higher, even the autoxidation scheme fails to reproduce the HO_2 observations. In this case the simulation in which the rate coefficient of RO_2-$R'O_2$ reactions was increased close to the collision limit shows a much better agreement compared to both the base case and the autoxidation case.

3.5 HO_x chemistry during CYPHEX: production and loss estimates

Using the optimal scenario from our model results, i.e. the one in which all measured species are included in the model (case III, Fig. 3), we have studied different processes impact-

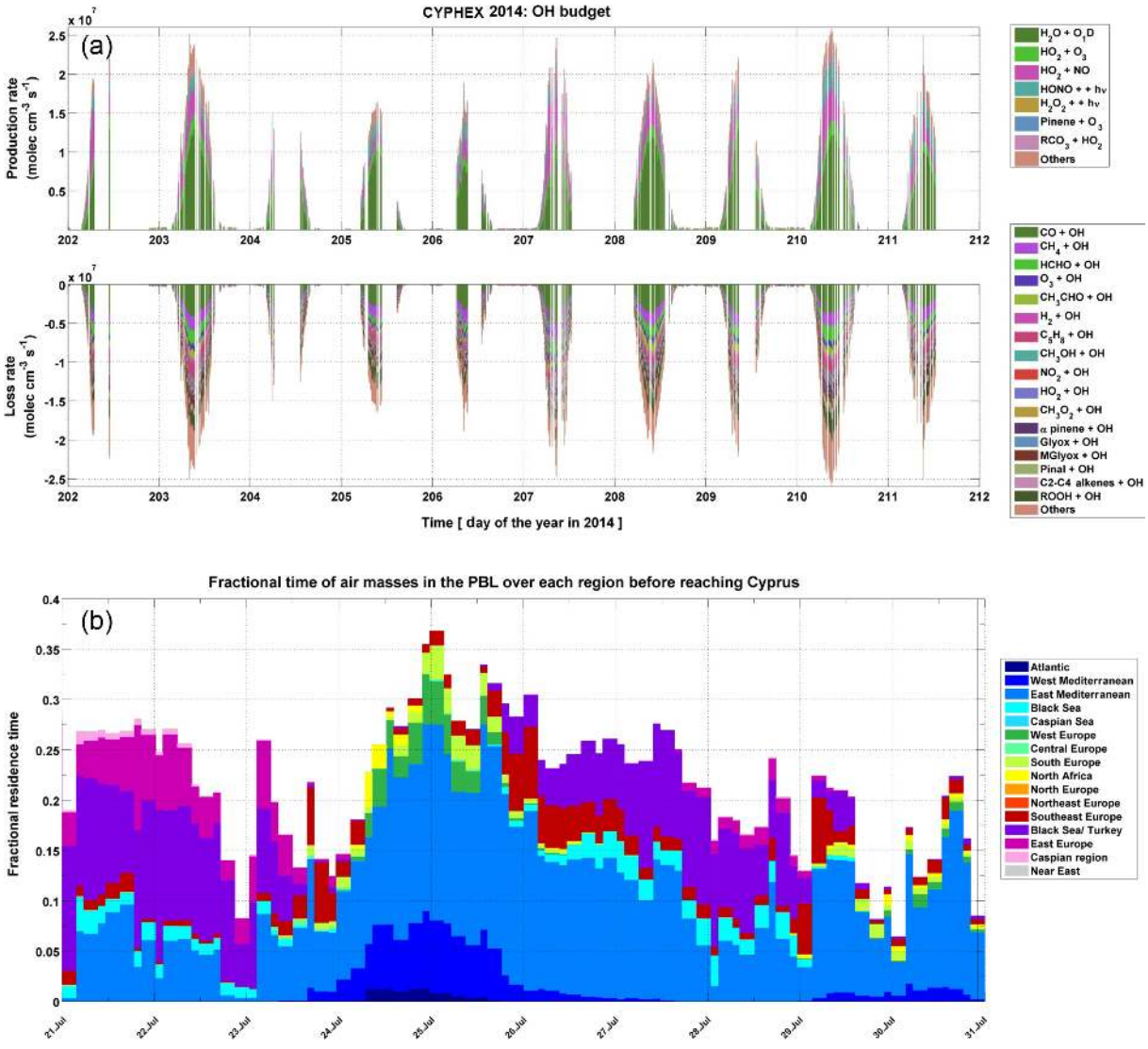

Figure 7. (a) Budget analysis for OH during CYPHEX. The HO_x budget is significantly impacted by the changes in air mass source regions. **(b)** FLEXPART evaluation of the contribution of different source regions within the planetary boundary layer to the air mass origin at the measurement site in Cyprus is shown in **(b)**. The air mass source regions are shown in a separate colour map (Fig. S1).

ing HO_x budgets. Since impact of terpene-generated RO_2 species was maximum on day 210 (29 July), we will ignore any special features on this day for our subsequent discussions using model case III, the terpene case. For CYPHEX, the major OH- as well as HO_x-producing channel is the reaction of atmospheric water vapour with O^1D generated from the photolysis of O_3 (Fig. 7). Peak daytime contributions of this channel towards OH production exceeded 45 % for most of the days and about 60 % on days 205, 208, and 209. The midday values coinciding with peak OH production on day 205 were marked by a conspicuous influence of aged air masses originating over southwestern Europe and considerably processed over the Mediterranean before reaching the site. The peak HO_2 values on this day were about 11 % lower than the average peak HO_2 values during the study period. The peak HO_2 value for $J(O^1D) > 2.5 \times 10^{-5}$ s^{-1} was 6.4×10^8 molec cm^{-3} for the study period while this value was only 5.7×10^8 molec cm^{-3} on day 205. While, on average, the recycled OH via reactions of HO_2 with NO and O_3 (Reactions R6–R7) contributed 33.6 % to the total OH production, this value was about 6 % lower for days 205–206. It may also be noted that although O_3 was very low on both days 205 and 206, with predominant influence of aged marine air, the contribution from $O^1D + H_2O$ to the total OH production still exceeded 50 %. Due to lower HONO mixing ratios, the fractional contributions of HONO photolysis towards peak OH production during midday on day 208 were significantly low at about 2.5 %–3.5 %. On all other

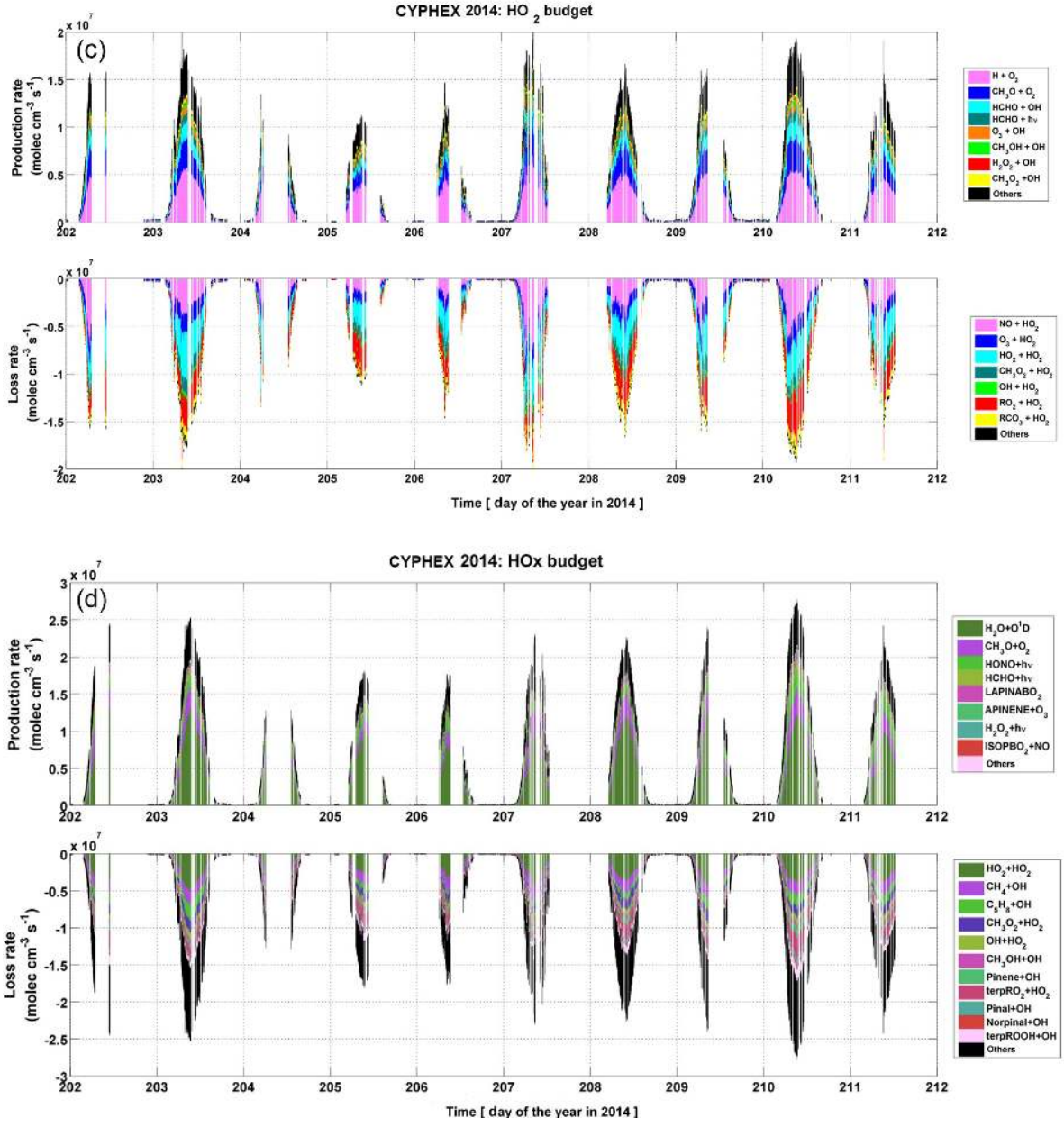

Figure 7. **(c)** Budget analysis for HO_2 and **(d)** budget analysis for HO_x, during CYPHEX. The descriptions for pinene, terpRO_2, and terpROOH are the same as in Fig. 5.

days, for which values are available, this channel contributed more than 6 % to peak OH production during noontime. The photolysis of HONO has the largest fractional contribution to the early morning OH production on day 211, reaching above 30 %. Overall during CYPHEX, the average daytime ($JO^1D > 0$) contribution to OH production from O_3 photolysis and subsequent reaction of O^1D with water vapour was about 39.1 %, the average daytime contribution from HONO photolysis was 12.3 %, and recycled OH from reaction of HO_2 with O_3 and NO accounts for 15.2 % and 18.4 % of the total OH production respectively. The four major OH-producing channels (Fig. 7) contribute up to 95 % of daytime OH production on most occasions, with 85.3 % on average. In addition, the reactions of acyl peroxy radicals (RCO_3) with HO_2 contribute about 3.1 % to the OH production, while the photolysis of H_2O_2 and the ozonolysis of pinene contribute 1.85 % and 2 % respectively.

The single major sink of OH during CYPHEX was CO, followed by CH_4, HCHO, C_5H_8, CH_3CHO, and O_3, on average accounting 20.9 %, 10.0 %, 7.8 %, 5.1 %, 4.9 %, and

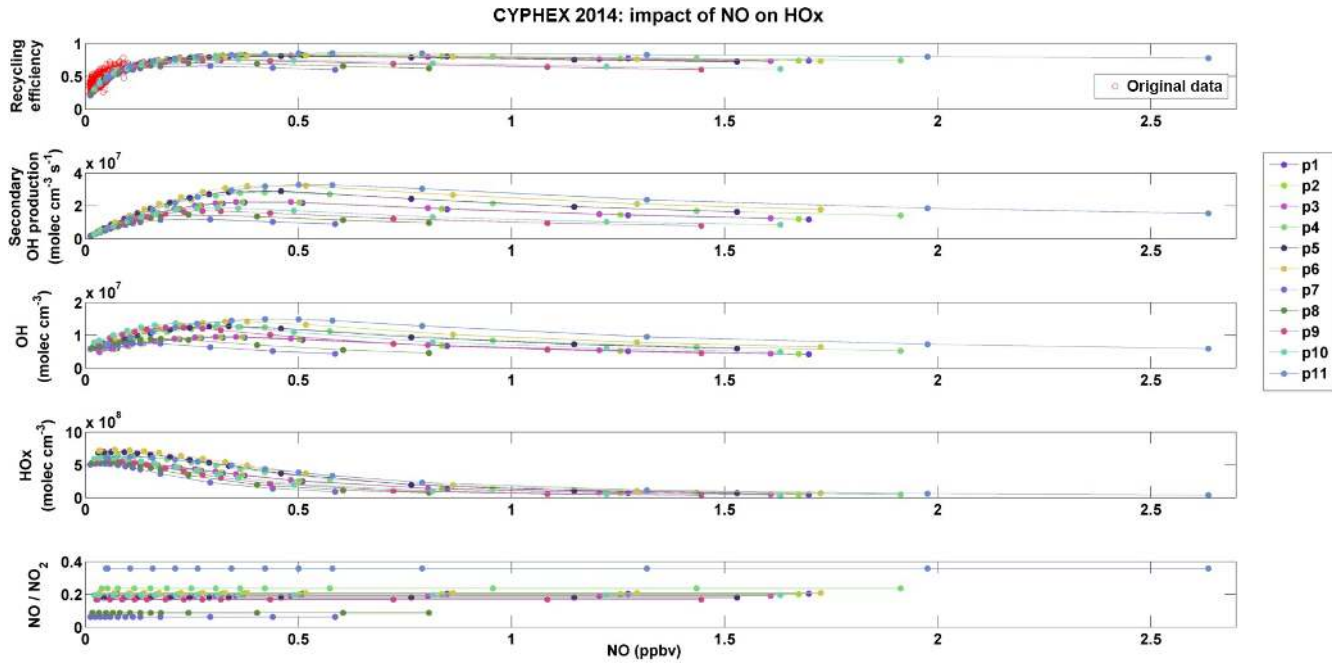

Figure 8. Sensitivity of recycling efficiency, secondary OH production, OH, and HO_x to changes in NO_x levels. P1–P11 are different starting points derived from the original dataset, for which NO_x is increased to 3 ppbv, while maintaining the original NO−NO_2 ratio.

4.1 % of OH losses respectively. The reactions of various peroxides with OH to form peroxy radicals, e.g. Reaction (R24), contribute 8.4 % to the OH loss. Further, oxidation of CH_3OH, pinal, C2–C4 alkenes, α-pinene, HO_2, NO_2, and CH_3O_2 by OH contributed 2.7 %, 2.4 %, 2.4 %, 2.2 %, 1.6 %, 1.4 %, and 1.4 % respectively. During days 205–206, the modelled OH loss (Fig. 7) as well as the calculated OH reactivity (Fig. 4) were the lowest of the study period. It is likely that the air masses arriving at the site during these days were already much processed, spending considerable time over the Atlantic and Mediterranean, leading to depleted OH reactivity. During this period of marine influence, the contribution of long-lived gases to the daytime OH loss increased by about 15 % while the contribution of shorter-lived gases like HCHO and CH_3CHO decreased by 34 % and 39 % respectively. HCHO concentrations are observed to be lowest between days 205 and 206, when the marine influence was the highest. The average lifetime of HCHO for the study period is calculated to be 0.86 days, and its concentrations are higher whenever air masses are influenced by southeastern Europe/Black Sea region.

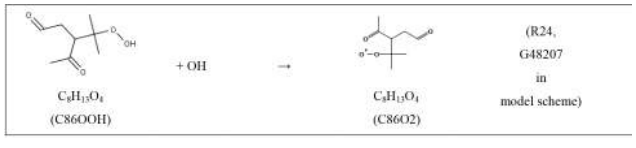

The major source of HO_2 during CYPHEX was the oxidation of CO by OH, contributing on average 36.2 % of daytime HO_2 production values. On days 205 and 206, when the site experienced aged oceanic air masses and CO concentrations were the lowest of the study period, the peak contribution of CO to daytime HO_2 production was still about 40.4 %. This shows that the contribution from other HO_2 precursors like HCHO decreases much faster than CO because of their shorter lifetime as the air mass passes over the ocean, and because they are isolated from their emission sources. The contributions of HCHO towards HO_2 production varied between 8 % and 23 % with an average daytime contribution of 15.6 % and included oxidation via both OH and photolysis. The methoxy radical (CH_3O), formed during oxidation of CH_4 and CH_3O_2, was also a significant source of HO_2, with peak contributions reaching 23 % on some occasions and an average daytime contribution of 17.8 %. On average, the reactions of HO_2 with NO and O_3, recycling OH, contributed 23.3 % and 18.2 % respectively towards daytime loss for HO_2. HO_2 losses by its self-reactions and reactions with CH_3O_2 reached peak daytime values of over 40 % and on average accounted for 30.3 % of daytime HO_2 losses. Among these, the major contribution was from the HO_2 self-reactions, with peak values of over 30 % during most days and average values of 22.4 %. The reactions of peroxy radicals (RO_2 and RCO_3) with HO_2 contribute 24.6 % to the HO_2 radical loss, resulting in increased under-prediction of HO_2 by the model with increasing terpene concentrations (Fig. S6). HO_2 losses due to recycling via NO and O_3 and the HO_2 losses via reactions with itself and CH_3O_2 are complementary during a diurnal cycle. The self-reactions gain in importance and peak around midday as the peroxy radi-

cal concentrations increase with increasing photochemistry, while recycling reactions dominate during periods with a larger solar zenith angle. During CYPHEX, for small solar zenith angles with $J(O^1D) > 2 \times 10^{-5}\ s^{-1}$, the contribution of recycling and self-reactions to HO_2 loss was 36.2 % and 32.7 % respectively. Overall, it is found that the lowest HO_x production and losses occurred in the highly processed air masses influenced by the marine boundary layer, mostly over the Mediterranean Sea, but sometimes as far as the Atlantic Ocean (days 205–206), with some influence from southwestern Europe/northern Africa (Fig. 7b and d).

3.6 Impact of NO_x levels on HO_x cycling

The close proximity of Cyprus to several countries with different socio-economic conditions makes its air quality vulnerable to the increases or decreases in primary and secondary air pollutants in one of these countries in Europe, Asia, and Africa. For example, increased NO_x emissions in one of the southern European countries or high CO from forest fires in Ukraine can be quickly transported to Cyprus in a matter of hours to days and modulate the atmospheric processing over the region. Increased NO_x emissions can impact the O_3–NO_x–VOC chemistry by changing the HO_x cycling. Even though the study period was characterized by NO of mostly less than 100 pptv, decreasing NO_x by 30 % still decreased OH levels by 14 %, these impacts being higher in the early morning and late afternoon. Conversely, increasing NO by 5 and 10 times caused 44 % and 70 % average enhancement in OH levels.

Because of its important role in O_3 production, NO_x emissions have been the focus of air quality investigations during preceding decades. Apart from their crucial role in O_3 production, NO_x levels also play a significant role in the self-cleaning capacity of the atmosphere due to their reactions with atmospheric HO_2 and RO_2. We test the impact of mainland Europe NO_x emissions on the self-cleaning capability of the climatically vulnerable Mediterranean atmosphere using the CYPHEX dataset. The recycling efficiency for OH (REf-OH) is defined as the ratio of OH produced from secondary sources via reactions of HO_2 with NO and O_3 (Reactions R6–R7) to the OH produced from primary and secondary sources. The primary sources of OH considered in our calculation include reaction of H_2O with O^1D produced from O_3 photolysis and the photolysis of HONO, H_2O_2, and organic peroxides. The contribution of the primary OH production from HONO photolysis is corrected by subtracting off the contribution from the recombination reaction of OH with NO.

While the present study is limited to NO < 100 pptv, modelling results show that REf-OH increases with an increase in NO levels (Fig. 8). The REf-OH increases from 0.28 at 10 pptv of NO to 0.42 at around 30 pptv of NO to 0.7 at 100 pptv of NO (Fig. 8). The REf-OH of 0.7 corresponds to a chain length of 2.8. The relationship of REf-OH with NO indicates that at higher NO (not observed for the CYPHEX data), the REf-OH would increase further. To understand if REf-OH would reach runaway conditions or saturate at a particular value, we chose several points along the REf–OH–NO curve and for each of these points, and we generated a hypothetical input dataset keeping all parameters constant but changing the NO_x levels from 0.2 to 3 ppbv, while maintaining the original NO/NO_2 ratio (Fig. 8).

Figure 8 shows that in general the REf-OH increases to about 0.85 at 500 pptv of NO. After this, it decreases gradually, related to the reaction of NO_2 with OH. Concurrently, the loss of HO_2 due to self-reactions and reaction of HO_2 with CH_3O_2 becomes much weaker compared to the loss of HO_2 to NO with increasing NO levels. The ratio of HO_2 losses via the radical–radical interactions (i.e. the reactions of HO_2 with HO_2 and CH_3O_2) to the HO_2 losses via the recycling channel (i.e. reactions of HO_2 with NO and O_3) decreases exponentially, becoming less than 1 at 35 pptv of NO and less than 0.5 at 70 pptv of NO and 0.01 at 1 ppbv NO. The secondary OH production also shows a similar pattern with respect to REf-OH, peaking around 500 pptv for the different input datasets and decaying thereafter. The model generated OH peaks in this range but the HO_x concentrations start to drop much earlier, from around 70 pptv of NO. At these low NO levels, HO_x loss by peroxide–peroxide reactions is comparable to the channels recycling HO_2 into OH, which can then be removed through reaction, e.g. with NO_2. However, the recycling efficiency is only about 0.6 at 70 pptv of NO. Budget analysis indicates that HO_x production drops with increasing NO levels for this test dataset constrained to specific NO_x levels. Overall, for the HC levels observed during CYPHEX, the self-cleaning capacity of the atmosphere peaks at around 500 pptv of NO, which at a NO / NO_2 ratio of 0.2 is equivalent to about 3.0 ppbv NO_x. Increasing NO_x emissions further would lead to decreased HO_x levels and the recycling efficiency is unlikely to increase further. Conversely, decreasing NO levels below a few hundred parts per trillion by volume of NO would also decrease the recycling efficiency for the same HC levels, indicating that a small amount of NO_x helps sustain the self-cleaning capacity of the atmosphere (Fig. 8).

4 Conclusions

Atmospheric OH and HO_2 were measured as part of a comprehensive atmospheric chemistry field measurement campaign conducted in Cyprus in the summer of 2014 to study the major processes impacting atmospheric oxidation and air chemistry in a relatively unpolluted coastal region, periodically influenced by long-range transport of European emissions. A comprehensive suite of atmospheric chemistry measurements obtained during CYPHEX enabled a detailed investigation of atmospheric oxidation processes, using a photochemical box model, under low-NO_x conditions. The

box model (CAABA/MECCA with MOM chemistry) simulations for OH agreed to within 10 % with in situ OH observations. Model simulations for HO_2 agreed to within 17 % of the in situ observations. However, the model strongly under-predicted HO_2 at high terpene (α- and β-pinene, limonene) concentrations (> 80 pptv), this under-prediction reaching up to 38 % at the highest terpene levels due to loss of HO_2 by reactions with terpene-generated peroxy radicals. Comparison of alternative reaction pathways to reduce this unrealistic HO_2 loss showed that autoxidation can be an effective sink for the RO_2 species generated from terpene oxidation. However, low-terpene and low-NO regimes, prevailing during CYPHEX, and the absence of limonene chemistry in the current model scheme, precluded a more rigorous analysis of the probable chemical pathways for RO_2 degradation in the atmosphere. Further, there is evidence that the rate constant of CH_3O_2 with OH could be 2 times faster than used in the current models (Bossolasco et al., 2014). Applying this in general to other peroxides, the rate constants need to be revisited as they will have a non-negligible impact on the chemical composition of the atmosphere, especially in remote low-NO_x environments where the peroxide lifetimes are relatively long. As already indicated in literature, there is large uncertainty in the rate coefficients of different RO_2 species with NO and HO_2 (King et al., 2001), which are scopes for future studies.

The radical budget analysis for CYPHEX showed that primary production of OH via photolysis of O_3 constituted the main OH source, and peak daytime contributions from this channel exceeded 45 % for most of the days. The average daytime contribution from HONO photolysis was 12.3 % but it exceeded 30 % in the early morning on a few occasions. The recycled OH from reaction of HO_2 with O_3 and NO accounted for 14.5 % and 17.7 % of the total OH production respectively. The maximum observed recycling efficiency was about 0.7 for about 100 pptv of NO. CO was not only the single major daytime sink of OH, accounting for nearly one-fifth of OH loss during the study period, but also the single major HO_2 production source. Despite low-NO_x regimes during CYPHEX, NO contributed more than 23 % of peak daytime loss for HO_2, reaching over 50 % on a few occasions. The lowest HO_x production and losses occurred in the highly processed air masses with low OH reactivity, i.e. low precursor levels. These air masses were heavily influenced by the marine boundary layer, mostly by the Mediterranean Sea, but sometimes as far as the Atlantic Ocean (24–25 July, days 205–206 of the year) with some influence from southwestern Europe/northern Africa. Additionally, our results connote the need for deeper understanding of the reaction channels for organic peroxides in the atmosphere.

Data availability. Data are available at the EDMOND repository of the Max Planck Society (Mallik et al., 2018). If further information is needed, please send an email to hartwig.harder@mpic.de.

The Supplement related to this article is available online at https://doi.org/10.5194/acp-18-10825-2018-supplement.

Author contributions. CM and HH conceptualized and wrote the paper. CM, HH, MM, AN, and LT conducted the OH and HO_2 measurements. EB, BD, CS, SK, and JW conducted the hydrocarbon and reactivity measurements. GJP, JS, and JNC conducted the SO_2 and radiation measurements. SH, AR, and HF carried out the measurements of HCHO and peroxides. HM and HS carried out the HONO measurements. CM, RS, DT, UJ, and AP contributed to the modelling efforts. IH carried out the FLEXPART simulations. JL contributed to writing the paper and designed the CYPHEX campaign.

Competing interests. The authors declare that they have no conflict of interest.

Acknowledgements. We acknowledge the contribution of the entire CYPHEX team, especially those members whose names are not listed as co-authors, for the success of the CYPHEX campaign. We also acknowledge the administrative and logistic support provided by the Cyprus Institute and the officials at the army base at Inea. We sincerely acknowledge the technical support provided by the workshop and electronics department in the Max Planck Institute for Chemistry in preparation for the campaign. Further, technical help from Markus Rudolf, Korbinian Hens, Cheryl Ernest, and Pippa Jones during preparation stage of the campaign is highly appreciated. We thank the handling editor and the two anonymous reviewers for their constructive comments and suggestions that have greatly improved the quality of this paper.

The article processing charges for this open-access publication were covered by the Max Planck Society.

Edited by: Neil M. Donahue
Reviewed by: two anonymous referees

References

Atkinson, R., Baulch, D. L., Cox, R. A., Hampson, R. F., Kerr, J. A., Rossi, M. J., Troe, J., and Evaluation, I. S. G. K. D.: Evaluated kinetic and photochemical data for atmospheric chemistry, organic species: Supplement VII, J. Phys. Chem. Ref. Data, 28, 191–393, https://doi.org/10.1063/1.556048, 1999.

Berresheim, H., Plass-Dülmer, C., Elste, T., Mihalopoulos, N., and Rohrer, F.: OH in the coastal boundary layer of Crete during MINOS: Measurements and relationship with ozone photolysis, Atmos. Chem. Phys., 3, 639–649, https://doi.org/10.5194/acp-3-639-2003, 2003.

Bossolasco, A., Farago, E. P., Schoemaecker, C., and Fittschen, C.: Rate constant of the reaction between CH_3O_2 and OH radicals, Chem. Phys. Lett., 593, 7–13, https://doi.org/10.1016/j.cplett.2013.12.052, 2014.

Boyd, A. A., Lesclaux, R., Jenkin, M. E., and Wallington, T. J.: A spectroscopic, kinetic, and product study of the (CH3)(2)C(OH)CH2O2 radical self-reaction and reaction with HO_2, J. Phys. Chem-Us, 100, 6594–6603, https://doi.org/10.1021/jp953292c, 1996.

Brune, W. H., Stevens, P. S., and Mather, J. H.: Measuring Oh and Ho2 in the Troposphere by Laser-Induced Fluorescence at Low-Pressure, J. Atmos. Sci., 52, 3328–3336, https://doi.org/10.1175/1520-0469(1995)052<3328:Moahit>2.0.Co;2, 1995.

Cabrera-Perez, D., Taraborrelli, D., Sander, R., and Pozzer, A.: Global atmospheric budget of simple monocyclic aromatic compounds, Atmos. Chem. Phys., 16, 6931–6947, https://doi.org/10.5194/acp-16-6931-2016, 2016.

Calogirou, A., Larsen, B. R., and Kotzias, D.: Gas-phase terpene oxidation products: a review, Atmos. Environ., 33, 1423–1439, https://doi.org/10.1016/S1352-2310(98)00277-5, 1999.

Capouet, M., Müller, J. F., Ceulemans, K., Compernolle, S., Vereecken, L., and Peeters, J.: Modeling aerosol formation in alpha-pinene photo-oxidation experiments, J. Geophys. Res., 113, D02308, https://doi.org/10.1029/2007JD008995, 2008.

Carslaw, N., Creasey, D. J., Harrison, D., Heard, D. E., Hunter, M. C., Jacobs, P. J., Jenkin, M. E., Lee, J. D., Lewis, A. C., Pilling, M. J., Saunders, S. M., and Seakins, P. W.: OH and HO_2 radical chemistry in a forested region of north-western Greece, Atmos. Environ., 35, 4725–4737, https://doi.org/10.1016/S1352-2310(01)00089-9, 2001.

Crosley, D. R.: The Measurement of Oh and Ho2 in the Atmosphere, J. Atmos. Sci., 52, 3299–3314, https://doi.org/10.1175/1520-0469(1995)052<3299:Tmooah>2.0.Co;2, 1995.

Crounse, J. D., Nielsen, L. B., Jorgensen, S., Kjaergaard, H. G., and Wennberg, P. O.: Autoxidation of Organic Compounds in the Atmosphere, J. Phys. Chem. Lett., 4, 3513–3520, https://doi.org/10.1021/jz4019207, 2013.

Derstroff, B., Hüser, I., Bourtsoukidis, E., Crowley, J. N., Fischer, H., Gromov, S., Harder, H., Janssen, R. H. H., Kesselmeier, J., Lelieveld, J., Mallik, C., Martinez, M., Novelli, A., Parchatka, U., Phillips, G. J., Sander, R., Sauvage, C., Schuladen, J., Stönner, C., Tomsche, L., and Williams, J.: Volatile organic compounds (VOCs) in photochemically aged air from the eastern and western Mediterranean, Atmos. Chem. Phys., 17, 9547–9566, https://doi.org/10.5194/acp-17-9547-2017, 2017.

Doche, C., Dufour, G., Foret, G., Eremenko, M., Cuesta, J., Beekmann, M., and Kalabokas, P.: Summertime tropospheric-ozone variability over the Mediterranean basin observed with IASI, Atmos. Chem. Phys., 14, 10589–10600, https://doi.org/10.5194/acp-14-10589-2014, 2014.

European Union emission inventory report 1990–2015 under the UNECE Convention on Long-range Transboundary Air Pollution (LRTAP), available at: https://www.eea.europa.eu/publications/annual-eu-emissions-inventory-report; http://www.eea.europa.eu/data-and-maps/data/data-viewers/air-emissions-viewer-lrtap, last access: 28 December 2017.

Evans, M. J., Shallcross, D. E., Law, K. S., Wild, J. O. F., Simmonds, P. G., Spain, T. G., Berrisford, P., Methven, J., Lewis, A. C., McQuaid, J. B., Pilling, M. J., Bandy, B. J., Penkett, S. A., and Pyle, J. A.: Evaluation of a Lagrangian box model using field measurements from EASE (Eastern Atlantic Summer Experiment) 1996, Atmos. Environ., 34, 3843–3863, https://doi.org/10.1016/S1352-2310(00)00184-9, 2000.

Fischer, H., Pozzer, A., Schmitt, T., Jöckel, P., Klippel, T., Taraborrelli, D., and Lelieveld, J.: Hydrogen peroxide in the marine boundary layer over the South Atlantic during the OOMPH cruise in March 2007, Atmos. Chem. Phys., 15, 6971–6980, https://doi.org/10.5194/acp-15-6971-2015, 2015.

Fuchs, H., Bohn, B., Hofzumahaus, A., Holland, F., Lu, K. D., Nehr, S., Rohrer, F., and Wahner, A.: Detection of HO_2 by laser-induced fluorescence: calibration and interferences from RO_2 radicals, Atmos. Meas. Tech., 4, 1209–1225, https://doi.org/10.5194/amt-4-1209-2011, 2011.

Gros, V., Williams, J., van Aardenne, J. A., Salisbury, G., Hofmann, R., Lawrence, M. G., von Kuhlmann, R., Lelieveld, J., Krol, M., Berresheim, H., Lobert, J. M., and Atlas, E.: Origin of anthropogenic hydrocarbons and halocarbons measured in the summertime european outflow (on Crete in 2001), Atmos. Chem. Phys., 3, 1223–1235, https://doi.org/10.5194/acp-3-1223-2003, 2003.

Hard, T. M., Obrien, R. J., Chan, C. Y., and Mehrabzadeh, A. A.: Tropospheric Free-Radical Determination by Fage, Environ. Sci. Technol., 18, 768–777, https://doi.org/10.1021/es00128a009, 1984.

Heland, J., Ziereis, H., Schlager, H., de Reus, M., Traub, M., Lelieveld, J., Roelofs, G.-J., Stock, P., and Roiger, A.: Aircraft measurements of nitrogen oxides, ozone, and carbon monoxide during MINOS 2001: distributions and correlation analyses, Atmos. Chem. Phys. Discuss., 3, 1991–2026, https://doi.org/10.5194/acpd-3-1991-2003, 2003.

Hens, K., Novelli, A., Martinez, M., Auld, J., Axinte, R., Bohn, B., Fischer, H., Keronen, P., Kubistin, D., Nölscher, A. C., Oswald, R., Paasonen, P., Petäjä, T., Regelin, E., Sander, R., Sinha, V., Sipilä, M., Taraborrelli, D., Tatum Ernest, C., Williams, J., Lelieveld, J., and Harder, H.: Observation and modelling of HOx radicals in a boreal forest, Atmos. Chem. Phys., 14, 8723–8747, https://doi.org/10.5194/acp-14-8723-2014, 2014.

Hildebrandt, L., Kostenidou, E., Mihalopoulos, N., Worsnop, D. R., Donahue, N. M., and Pandis, S. N.: Formation of highly oxygenated organic aerosol in the atmosphere: Insights from the Finokalia Aerosol Measurement Experiments, Geophys. Res. Lett., 37, L23801, https://doi.org/10.1029/2010gl045193, 2010.

Hosaynali Beygi, Z., Fischer, H., Harder, H. D., Martinez, M., Sander, R., Williams, J., Brookes, D. M., Monks, P. S., and Lelieveld, J.: Oxidation photochemistry in the Southern Atlantic boundary layer: unexpected deviations of photochemical steady state, Atmos. Chem. Phys., 11, 8497–8513, https://doi.org/10.5194/acp-11-8497-2011, 2011.

Hüser, I., Harder, H., Heil, A., and Kaiser, J. W.: Assumptions about footprint layer heights influence the quantification of emission sources: a case study for Cyprus, Atmos. Chem. Phys., 17, 10955–10967, https://doi.org/10.5194/acp-17-10955-2017, 2017.

IUPAC: Task Group on Atmospheric Chemical Kinetic Data Evaluation, Ammann, M., Cox, R. A., Crowley, J. N., Jenkin, M. E., Mellouki, A., Rossi, M. J., Troe, J., and Wallington, T. J., available at: http://iupac.pole-ether.fr/index.html (last access: 28 December 2017), 2015.

Jenkin, M. E., Saunders, S. M., and Pilling, M. J.: The tropospheric degradation of volatile organic compounds: A proto-

col for mechanism development, Atmos. Environ., 31, 81–104, https://doi.org/10.1016/S1352-2310(96)00105-7, 1997.

Jenkin, M. E., Young, J. C., and Rickard, A. R.: The MCM v3.3.1 degradation scheme for isoprene, Atmos. Chem. Phys., 15, 11433–11459, https://doi.org/10.5194/acp-15-11433-2015, 2015.

Kalabokas, P. D., Cammas, J.-P., Thouret, V., Volz-Thomas, A., Boulanger, D., and Repapis, C. C.: Examination of the atmospheric conditions associated with high and low summer ozone levels in the lower troposphere over the eastern Mediterranean, Atmos. Chem. Phys., 13, 10339–10352, https://doi.org/10.5194/acp-13-10339-2013, 2013.

King, M. D., Canosa-Mas, C. E., and Wayne, R. P.: Gas-phase reactions between RO_2 and NO, HO_2 or CH_3O_2: correlations between rate constants and the SOMO energy of the peroxy (RO2) radical, Atmos. Environ., 35, 2081–2088, https://doi.org/10.1016/S1352-2310(00)00501-X, 2001.

Kleanthous, S., Vrekoussis, M., Mihalopoulos, N., Kalabokas, P., and Lelieveld, J.: On the temporal and spatial variation of ozone in Cyprus, Sci. Total Environ., 476, 677–687, https://doi.org/10.1016/j.scitotenv.2013.12.101, 2014.

Knote, C., Tuccella, P., Curci, G., Emmons, L., Orlando, J. J., Madronich, S., Baro, R., Jimenez-Guerrero, P., Luecken, D., Hogrefe, C., Forkel, R., Werhahn, J., Hirtl, M., Perez, J. L., San Jose, R., Giordano, L., Brunner, D., Yahya, K., and Zhang, Y.: Influence of the choice of gas-phase mechanism on predictions of key gaseous pollutants during the AQMEII phase-2 intercomparison, Atmos. Environ., 115, 553–568, https://doi.org/10.1016/j.atmosenv.2014.11.066, 2015.

Kormann, R., Fischer, H., de Reus, M., Lawrence, M., Brühl, Ch., von Kuhlmann, R., Holzinger, R., Williams, J., Lelieveld, J., Warneke, C., de Gouw, J., Heland, J., Ziereis, H., and Schlager, H.: Formaldehyde over the eastern Mediterranean during MINOS: Comparison of airborne in-situ measurements with 3D-model results, Atmos. Chem. Phys., 3, 851–861, https://doi.org/10.5194/acp-3-851-2003, 2003.

Lee, J. D., Young, J. C., Read, K. A., Hamilton, J. F., Hopkins, J. R., Lewis, A. C., Bandy, B. J., Davey, J., Edwards, P., Ingham, T., Self, D. E., Smith, S. C., Pilling, M. J., and Heard, D. E.: Measurement and calculation of OH reactivity at a United Kingdom coastal site, J. Atmos. Chem., 64, 53–76, https://doi.org/10.1007/s10874-010-9171-0, 2009.

Lelieveld, J. and Dentener, F. J.: What controls tropospheric ozone?, J. Geophys. Res.-Atmos., 105, 3531–3551, https://doi.org/10.1029/1999jd901011, 2000.

Lelieveld, J., Berresheim, H., Borrmann, S., Crutzen, P. J., Dentener, F. J., Fischer, H., Feichter, J., Flatau, P. J., Heland, J., Holzinger, R., Korrmann, R., Lawrence, M. G., Levin, Z., Markowicz, K. M., Mihalopoulos, N., Minikin, A., Ramanathan, V., de Reus, M., Roelofs, G. J., Scheeren, H. A., Sciare, J., Schlager, H., Schultz, M., Siegmund, P., Steil, B., Stephanou, E. G., Stier, P., Traub, M., Warneke, C., Williams, J., and Ziereis, H.: Global air pollution crossroads over the Mediterranean, Science, 298, 794–799, https://doi.org/10.1126/science.1075457, 2002.

Lelieveld, J., Dentener, F. J., Peters, W., and Krol, M. C.: On the role of hydroxyl radicals in the self-cleansing capacity of the troposphere, Atmos. Chem. Phys., 4, 2337–2344, https://doi.org/10.5194/acp-4-2337-2004, 2004.

Lelieveld, J., Hadjinicolaou, P., Kostopoulou, E., Chenoweth, J., El Maayar, M., Giannakopoulos, C., Hannides, C., Lange, M. A., Tanarhte, M., Tyrlis, E., and Xoplaki, E.: Climate change and impacts in the Eastern Mediterranean and the Middle East, Clim. Change, 114, 667–687, https://doi.org/10.1007/s10584-012-0418-4, 2012.

Lelieveld, J., Evans, J. S., Fnais, M., Giannadaki, D., and Pozzer, A.: The contribution of outdoor air pollution sources to premature mortality on a global scale, Nature, 525, 367–371, https://doi.org/10.1038/nature15371, 2015.

Lelieveld, J., Gromov, S., Pozzer, A., and Taraborrelli, D.: Global tropospheric hydroxyl distribution, budget and reactivity, Atmos. Chem. Phys., 16, 12477–12493, https://doi.org/10.5194/acp-16-12477-2016, 2016.

Levy, H.: Normal Atmosphere – Large Radical and Formaldehyde Concentrations Predicted, Science, 173, 141–143, https://doi.org/10.1126/science.173.3992.141, 1971.

Lew, M. M., Dusanter, S., and Stevens, P. S.: Measurement of interferences associated with the detection of the hydroperoxy radical in the atmosphere using laser-induced fluorescence, Atmos. Meas. Tech., 11, 95–109, https://doi.org/10.5194/amt-11-95-2018, 2018.

Lewis, A. C., Hopkins, J. R., Carpenter, L. J., Stanton, J., Read, K. A., and Pilling, M. J.: Sources and sinks of acetone, methanol, and acetaldehyde in North Atlantic marine air, Atmos. Chem. Phys., 5, 1963–1974, https://doi.org/10.5194/acp-5-1963-2005, 2005.

Li, J. S., Reiffs, A., Parchatka, U., and Fischer, H.: *In Situ* Measurements of Atmospheric Co and Its Correlation with Nox and O-3 at a Rural Mountain Site, Metrol. Meas. Syst., 22, 25–38, 2015.

Librando, V. and Tringali, G.: Atmospheric fate of OH initiated oxidation of terpenes. Reaction mechanism of alpha-pinene degradation and secondary organic aerosol formation, J. Environ. Manage., 75, 275–282, https://doi.org/10.1016/j.jenvman.2005.01.001, 2005.

Mao, J., Ren, X., Brune, W. H., Olson, J. R., Crawford, J. H., Fried, A., Huey, L. G., Cohen, R. C., Heikes, B., Singh, H. B., Blake, D. R., Sachse, G. W., Diskin, G. S., Hall, S. R., and Shetter, R. E.: Airborne measurement of OH reactivity during INTEX-B, Atmos. Chem. Phys., 9, 163–173, https://doi.org/10.5194/acp-9-163-2009, 2009.

Mallik, C., Bourtsoukidis, E., Crowley, J. N., Derstroff, B., Fischer, H., Hafermann, S., Martinez, M., Meusel, H., Novelli, A., Phillips, G. J., Reiffs, A., Sauvage, C., Schuladen, J., Su, H., Tomsche, L., Williams, J., and Harder, H.; CYprus PHotochemistry EXperiment HO_x measurements and modelling, Max Planck Society, https://doi.org/10.17617/3.1n, last access: 5 July 2018.

Martinez, M., Harder, H., Kubistin, D., Rudolf, M., Bozem, H., Eerdekens, G., Fischer, H., Klüpfel, T., Gurk, C., Königstedt, R., Parchatka, U., Schiller, C. L., Stickler, A., Williams, J., and Lelieveld, J.: Hydroxyl radicals in the tropical troposphere over the Suriname rainforest: airborne measurements, Atmos. Chem. Phys., 10, 3759–3773, https://doi.org/10.5194/acp-10-3759-2010, 2010.

Mauldin, R. L., Berndt, T., Sipila, M., Paasonen, P., Petaja, T., Kim, S., Kurten, T., Stratmann, F., Kerminen, V. M., and Kulmala, M.: A new atmospherically relevant oxidant of sulphur dioxide, Nature, 488, 193–196, https://doi.org/10.1038/nature11278, 2012.

Meusel, H., Kuhn, U., Reiffs, A., Mallik, C., Harder, H., Martinez, M., Schuladen, J., Bohn, B., Parchatka, U., Crowley, J. N., Fischer, H., Tomsche, L., Novelli, A., Hoffmann, T., Janssen, R. H. H., Hartogensis, O., Pikridas, M., Vrekoussis, M., Bourtsoukidis, E., Weber, B., Lelieveld, J., Williams, J., Pöschl, U., Cheng, Y., and Su, H.: Daytime formation of nitrous acid at a coastal remote site in Cyprus indicating a common ground source of atmospheric HONO and NO, Atmos. Chem. Phys., 16, 14475–14493, https://doi.org/10.5194/acp-16-14475-2016, 2016.

Nguyen, T. B., Crounse, J. D., Teng, A. P., Clair, J. M. S., Paulot, F., Wolfe, G. M., and Wennberg, P. O.: Rapid deposition of oxidized biogenic compounds to a temperate forest, P. Natl. Acad. Sci. USA, 112, E392–E401, https://doi.org/10.1073/pnas.1418702112, 2015.

Nguyen, T. L., Peeters, J., and Vereecken, L.: Theoretical study of the gas-phase ozonolysis of b-pinene (C10H16), Phys. Chem. Chem. Phys., 11, 5643–5656, https://doi.org/10.1039/b822984h, 2009.

Nolscher, A., Butler, T., Auld, J., Veres, P., Muñoz, A., Taraborrelli, D., Vereecken, L., Lelieveld, J., and Williams, J.: Using total OH reactivity to assess isoprene photooxidation via measurement and model, Atmos. Environ., 89, 453–463, https://doi.org/10.1016/j.atmosenv.2014.02.024, 2014.

Novelli, A., Hens, K., Tatum Ernest, C., Kubistin, D., Regelin, E., Elste, T., Plass-Dülmer, C., Martinez, M., Lelieveld, J., and Harder, H.: Characterisation of an inlet pre-injector laser-induced fluorescence instrument for the measurement of atmospheric hydroxyl radicals, Atmos. Meas. Tech., 7, 3413–3430, https://doi.org/10.5194/amt-7-3413-2014, 2014a.

Novelli, A., Vereecken, L., Lelieveld, J., and Harder, H.: Direct observation of OH formation from stabilised Criegee intermediates, Phys. Chem. Chem. Phys., 16, 19941–19951, https://doi.org/10.1039/c4cp02719a, 2014b.

Peeters, J., Müller, J.-F., Stavrakou, T., and Nguyen, V. S.: 30 Hydroxyl radical recycling in isoprene oxidation driven by hydrogen bonding and hydrogen tunneling: the upgraded LIM1 mechanism, J. Phys. Chem. A, 118, 8625–8643, 2014.

Ren, X. R., Olson, J. R., Crawford, J. H., Brune, W. H., Mao, J. Q., Long, R. B., Chen, Z., Chen, G., Avery, M. A., Sachse, G. W., Barrick, J. D., Diskin, G. S., Huey, L. G., Fried, A., Cohen, R. C., Heikes, B., Wennberg, P. O., Singh, H. B., Blake, D. R., and Shetter, R. E.: HOx chemistry during INTEX-A 2004: Observation, model calculation, and comparison with previous studies, J. Geophys. Res.-Atmos., 113, D05310, https://doi.org/10.1029/2007jd009166, 2008.

Rickard, A. and Pascoe, S.: The Master Chemical Mechanism (MCM), available at: http://mcm.leeds.ac.uk/MCMv3.3.1/categories/saunders-2003-4_6_1-gen-master.htt?rxnId=6916 (last access: 28 December 2017), 2009.

Rohrer, F., Lu, K. D., Hofzumahaus, A., Bohn, B., Brauers, T., Chang, C. C., Fuchs, H., Haseler, R., Holland, F., Hu, M., Kita, K., Kondo, Y., Li, X., Lou, S. R., Oebel, A., Shao, M., Zeng, L. M., Zhu, T., Zhang, Y. H., and Wahner, A.: Maximum efficiency in the hydroxyl-radical-based self-cleansing of the troposphere, Nat. Geosci., 7, 559–563, https://doi.org/10.1038/Ngeo2199, 2014.

Salisbury, G., Williams, J., Holzinger, R., Gros, V., Mihalopoulos, N., Vrekoussis, M., Sarda-Estéve, R., Berresheim, H., von Kuhlmann, R., Lawrence, M., and Lelieveld, J.: Ground-based PTR-MS measurements of reactive organic compounds during the MINOS campaign in Crete, July–August 2001, Atmos. Chem. Phys., 3, 925–940, https://doi.org/10.5194/acp-3-925-2003, 2003.

Sander, R., Kerkweg, A., Jöckel, P., and Lelieveld, J.: Technical note: The new comprehensive atmospheric chemistry module MECCA, Atmos. Chem. Phys., 5, 445–450, https://doi.org/10.5194/acp-5-445-2005, 2005.

Sander, R., Baumgaertner, A., Gromov, S., Harder, H., Jöckel, P., Kerkweg, A., Kubistin, D., Regelin, E., Riede, H., Sandu, A., Taraborrelli, D., Tost, H., and Xie, Z.-Q.: The atmospheric chemistry box model CAABA/MECCA-3.0, Geosci. Model Dev., 4, 373–380, https://doi.org/10.5194/gmd-4-373-2011, 2011.

Sander, S. P., Abbatt, J., Barker, J. R., Burkholder, J. B., Friedl, R. R., Golden, D. M., Huie, R. E., Kolb, C. E., Kurylo, M. J., Moortgat, G. K., Orkin, V. L., and Wine, P. H.: Chemical Kinetics and Photochemical Data for Use in Atmospheric Studies, Evaluation No. 17, JPL Publication 10-6, Jet Propulsion Laboratory, Pasadena, available at: http://jpldataeval.jpl.nasa.gov (last access: 28 December 2017), 2011.

Sandu, A. and Sander, R.: Technical note: Simulating chemical systems in Fortran90 and Matlab with the Kinetic PreProcessor KPP-2.1, Atmos. Chem. Phys., 6, 187–195, https://doi.org/10.5194/acp-6-187-2006, 2006.

Silva, R. A., West, J. J., Zhang, Y. Q., Anenberg, S. C., Lamarque, J. F., Shindell, D. T., Collins, W. J., Dalsoren, S., Faluvegi, G., Folberth, G., Horowitz, L. W., Nagashima, T., Naik, V., Rumbold, S., Skeie, R., Sudo, K., Takemura, T., Bergmann, D., Cameron-Smith, P., Cionni, I., Doherty, R. M., Eyring, V., Josse, B., MacKenzie, I. A., Plummer, D., Righi, M., Stevenson, D. S., Strode, S., Szopa, S., and Zeng, G.: Global premature mortality due to anthropogenic outdoor air pollution and the contribution of past climate change, Environ. Res. Lett., 8, 034005, https://doi.org/10.1088/1748-9326/8/3/034005, 2013.

Sinha, V., Williams, J., Diesch, J. M., Drewnick, F., Martinez, M., Harder, H., Regelin, E., Kubistin, D., Bozem, H., Hosaynali-Beygi, Z., Fischer, H., André-Hernández, M. D., Kartal, D., Adame, J. A., and Lelieveld, J.: Constraints on instantaneous ozone production rates and regimes during DOMINO derived using in-situ OH reactivity measurements, Atmos. Chem. Phys., 12, 7269–7283, https://doi.org/10.5194/acp-12-7269-2012, 2012.

Smith, S. C., Lee, J. D., Bloss, W. J., Johnson, G. P., Ingham, T., and Heard, D. E.: Concentrations of OH and HO_2 radicals during NAMBLEX: measurements and steady state analysis, Atmos. Chem. Phys., 6, 1435–1453, https://doi.org/10.5194/acp-6-1435-2006, 2006.

Sobanski, N., Tang, M. J., Thieser, J., Schuster, G., Pöhler, D., Fischer, H., Song, W., Sauvage, C., Williams, J., Fachinger, J., Berkes, F., Hoor, P., Platt, U., Lelieveld, J., and Crowley, J. N.: Chemical and meteorological influences on the lifetime of NO_3 at a semi-rural mountain site during PARADE, Atmos. Chem. Phys., 16, 4867–4883, https://doi.org/10.5194/acp-16-4867-2016, 2016.

Stockwell, W. R., Kirchner, F., Kuhn, M., and Seefeld, S.: A new mechanism for regional atmospheric chemistry modeling, J. Geophys. Res.-Atmos., 102, 25847–25879, https://doi.org/10.1029/97jd00849, 1997.

Stohl, A., Forster, C., Frank, A., Seibert, P., and Wotawa, G.: Technical note: The Lagrangian particle dispersion model FLEXPART version 6.2, Atmos. Chem. Phys., 5, 2461–2474, https://doi.org/10.5194/acp-5-2461-2005, 2005.

Stone, D., Whalley, L. K., and Heard, D. E.: Tropospheric OH and HO2 radicals: field measurements and model comparisons, Chem. Soc. Rev., 41, 6348–6404, https://doi.org/10.1039/c2cs35140d, 2012.

Taraborrelli, D., Lawrence, M. G., Butler, T. M., Sander, R., and Lelieveld, J.: Mainz Isoprene Mechanism 2 (MIM2): an isoprene oxidation mechanism for regional and global atmospheric modelling, Atmos. Chem. Phys., 9, 2751–2777, https://doi.org/10.5194/acp-9-2751-2009, 2009.

Taraborrelli, D., Lawrence, M. G., Crowley, J. N., Dillon, T. J., Gromov, S., Gross, C. B. M., Vereecken, L., and Lelieveld, J.: Hydroxyl radical buffered by isoprene oxidation over tropical forests, Nat. Geosci., 5, 190–193, https://doi.org/10.1038/Ngeo1405, 2012.

Taraborrelli, D., Perez, D. C., Sander, R., and Pozzer, A.: Mainz Organics Mechanism (MOM): description and sensitivity to some estimated kinetic parameters, EGU General Assembly, Vienna, Austria, 12–17 April 2015, EGU2015-12026, available at: https://meetingorganizer.copernicus.org/EGU2015/EGU2015-12026.pdf (last access: 28 December 2017), 2015.

Thornton, J. A., Wooldridge, P. J., Cohen, R. C., Martinez, M., Harder, H., Brune, W. H., Williams, E. J., Roberts, J. M., Fehsenfeld, F. C., Hall, S. R., Shetter, R. E., Wert, B. P., and Fried, A.: Ozone production rates as a function of NO_x abundances and HOx production rates in the Nashville urban plume, J. Geophys. Res.-Atmos., 107, 4146, https://doi.org/10.1029/2001jd000932, 2002.

Tyrlis, E., Tymvios, F. S., Giannakopoulos, C., and Lelieveld, J.: The role of blocking in the summer 2014 collapse of Etesians over the eastern Mediterranean, J. Geophys. Res.-Atmos., 120, 6777–6792, https://doi.org/10.1002/2015jd023543, 2015.

Vereecken, L. and Peeters, J.: A theoretical study of the OH-initiated gas-phase oxidation mechanism of b-pinene (C10H16): first generation products, Phys. Chem. Chem. Phys., 14, 3802–3815, https://doi.org/10.1039/c2cp23711c, 2012.

Vereecken, L., Müller, J.-F., and Peeters, J.: Low-volatility poly-oxygenates in the OH-initiated atmospheric oxidation of a-pinene: impact of non-traditional peroxyl radical chemistry, Phys. Chem. Chem. Phys., 9, 5241–5248, https://doi.org/10.1039/b708023a, 2007.

Wisthaler, A., Jensen, N. R., Winterhalter, R., Lindinger, W., and Hjorth, J.: Measurements of acetone and other gas phase product yields from the OH-initiated oxidation of terpenes by proton-transfer-reaction mass spectrometry (PTR-MS), Atmos. Environ., 35, 6181–6191, https://doi.org/10.1016/S1352-2310(01)00385-5, 2001.

Yang, Y. D., Shao, M., Wang, X. M., Nolscher, A. C., Kessel, S., Guenther, A., and Williams, J.: Towards a quantitative understanding of total OH reactivity: A review, Atmos. Environ., 134, 147–161, https://doi.org/10.1016/j.atmosenv.2016.03.010, 2016.

Yarwood, G., Rao, S., Yocke, M., and Whitten, G.: Updates to the Carbon Bond Mechanism: CB05, Report to the U.S. Environmental Protection Agency, available at: http://www.camx.com/files/cb05_final_report_120805.aspx (last access: 28 December 2017), 2005.

Zhang, X., Mcvay, R. C., Huang, D. D., Dalleska, N. F., Aumont, B., Flagan, R. C., and Seinfeld, J. H.: Formation and evolution of molecular products in alpha-pinene secondary organic aerosol, P. Natl. Acad. Sci. USA, 112, 14168–14173, https://doi.org/10.1073/pnas.1517742112, 2015.